

# Spectra probing the number ratio of C- to M-type AGB stars in the NGC 6822 galaxy <sup>★, ★★</sup>

N. Kacharov<sup>1,2,3</sup>, M. Rejkuba<sup>1</sup>, and M.-R. L. Cioni<sup>4,5★★</sup>

<sup>1</sup> ESO, Karl-Schwarzschild-Strasse 2, D-85748 Garching, Germany

<sup>2</sup> Institute of Astronomy, Bulgarian Academy of Sciences, 72 Tsarigradsko Chaussee Blvd., 1784 Sofia, Bulgaria

<sup>3</sup> Department of Astronomy, St. Kliment Ohridski University of Sofia, 5 James Bourchier Blvd., 1164 Sofia, Bulgaria

<sup>4</sup> University Observatory Munich, Scheinerstrasse 1, 81679 München, Germany

<sup>5</sup> University of Hertfordshire, Physics Astronomy and Mathematics, Hatfield AL10 9AB, United Kingdom

Received: 31.05.2011 / Accepted: 16.10.2011

## ABSTRACT

**Aims.** We calibrate spectroscopically the C- versus (vs.) M-type asymptotic giant branch (AGB) star selection made using near-IR photometry, and investigate the spatial distribution of the C/M ratio in NGC 6822, based on low resolution spectroscopy and near-IR photometry.

**Methods.** We obtained low resolution multi-object spectroscopy with the VIMOS instrument at the ESO VLT of  $\sim 800$  stars in seven fields centred on NGC 6822. The spectroscopic classification of giant stars in NGC 6822 and foreground dwarf contaminants was made by comparing more than 500 good quality spectra with the spectroscopic atlas of Turnshek et al. (1985). The sample of spectroscopically confirmed AGB stars in NGC 6822 is divided into C- and M-rich giants to constrain the C vs. M AGB star selection criteria based on photometry. The larger near-IR photometric sample is then used to investigate the C/M ratio gradients across the galaxy.

**Results.** We present the largest catalogue of near-IR photometry and spectra of AGB stars in NGC 6822 with 150 C-stars and 122 M-stars. Seventy-nine percent of the C-stars in our catalogue are redder than  $(J - K)_0 = 1.2$  mag, and 12% are brighter than  $K_0 = 16.45$  mag and bluer than  $(J - K)_0 = 1.2$  mag. The remaining 9% are mixed with the M-type AGB stars, 88% of which have colours  $(J - H)_0 > 0.73$  mag and  $(J - K)_0$  between 0.9 mag and 1.2 mag. The remainder are mixed with dwarfs and C-type stars. The foreground dwarfs have preferably colours  $(J - H)_0 < 0.73$  mag (95%). Using the proposed criteria, we estimate that the overall C/M ratio of the galaxy is around 0.8 with a spread between  $0.2 < C/M < 1.8$ . These results suggest that the metallicity index  $[\text{Fe}/\text{H}]$  is between  $-1.2$  dex and  $-1.3$  dex according to the different calibrations and that there is a significant spread of about  $0.4 \div 0.6$  dex. We also discuss age rather than metallicity variations that could explain the C/M ratio trends.

**Key words.** Galaxies: irregular, dwarf galaxies, local group – Galaxies: Individual: NGC 6822 – Galaxies: stellar content – Stars: AGB stars, C- and M-type stars

## 1. Introduction

The intermediate-age asymptotic giant branch (AGB) stars are classified as carbon-rich (C stars) or oxygen-rich (M stars), depending on which element dominates their atmosphere. These stars are among the most luminous stars in a galaxy in near-IR, and are thus easily observable at large distances. The upcoming large telescopes ( $> 20$  m) will operate most efficiently in near-IR and will detect large samples of AGB stars in nearby galaxies. In Addition, this stellar evolutionary phase is extremely important to the studies of high redshift galaxies, because these relatively young galaxies contain significant fraction of intermediate-age stars, and in a 1 Gyr old simple stellar population up to 80% of the K-band light originates from the luminous AGB stars (Maraston 2005; Maraston et al. 2006). Nevertheless, the intermediate-age stellar evolutionary models,

the stellar atmospheres, the internal composition, and the physics of luminous AGB stars are all affected by large uncertainties (Cassisi et al. 2001; Gallart et al. 2005; Ventura & Marigo 2010), and currently this is one area of stellar evolutionary theory where important improvements are needed, both theoretically (Marigo & Girardi 2007; Marigo et al. 2008) and observationally (e.g. Girardi & Marigo 2007; Lyubenova et al. 2010; Girardi et al. 2010).

At present, the selection of C and M stars is made using either near-IR colour-magnitude diagrams or colour-colour diagrams for broad- and narrow-band filters (Battinelli & Demers 2004). These surveys rely on photometric selection criteria that have inherent uncertainties, do not easily distinguish K giants and Galactic M dwarfs, and do not account for S-type stars. The situation somewhat improves, at least for K giants, if optical and IR selection criteria are used together (Cioni & Habing 2005). The spectroscopic classification of AGB stars covering a range of metallicities is necessary to properly estimate the biases and establish quantitative criteria for the photometric selection boxes.

The C/M ratio is the number ratio of C-type (carbon-rich) to M-type (oxygen-rich) AGB stars. It is a function of the  $[\text{Fe}/\text{H}]$  abundance (Battinelli & Demers 2005) and provides a

Send offprint requests to: N. Kacharov, kacni@abv.bg

\* Based on observations made with ESO telescopes at the La Silla Paranal Observatory under programme ID 383.D-0367

\*\* Complete Table 2 and the reduced spectra in ASCII format are available at the CDS via anonymous ftp to cdsarc.u-strasbg.fr (130.79.128.5).

\*\*\* Research Fellow of the Alexander von Humboldt Foundation

simple indication of the metallicity distribution across galaxies (e.g. Cioni et al. 2008, 2009; Cioni & Habing 2003, for M 33 and the Magellanic Clouds, respectively). The C/M vs. [Fe/H] relation is due to the combined effect of pronounced carbon dredge-up on the stellar spectrum at low metallicity, and the blue colours of metal-poor red giants (Iben & Renzini 1983). The lower metallicity O-rich stars turn into C-type AGB stars more easily and remain so for a longer time than those of higher metallicity because fewer carbon atoms need to be dredged up to effect this transformation, and in addition at lower metallicity the AGB evolutionary tracks have higher temperatures, which causes lower abundances of TiO molecules, hence smaller numbers of M stars. However, while theoretically clear arguments exist for the dependence of C/M ratio on [Fe/H], the relation is still poorly calibrated owing to: (i) the ill-defined criteria for selecting C and M stars; (ii) the contamination from both foreground and S stars (S stars have equal amounts of carbon and oxygen in their atmospheres); and (iii) the need to have a well-defined sample of AGB stars with spectroscopically determined metallicities.

The NGC 6822 galaxy is an ideal target for the study of C- and M-type AGB stars and the C/M ratio as a function of metallicity. It is a relatively well-studied dwarf irregular galaxy in the constellation Sagittarius at a distance of  $\sim 490$  kpc (Mateo 1998). Owing to its low Galactic latitude ( $b = -18.39^\circ$ ), it is affected by moderate foreground extinction,  $E(B - V) = 0.24$  mag (Schlegel et al. 1998). It is similar in mass ( $1.9 \times 10^9 M_\odot$ ), structure, and metallicity ( $\sim 0.2 Z_\odot$ ) to the Small Magellanic Cloud and consists of different morphological components (disk, bar, and halo), rotation, gas content, active star formation, and dark matter distribution (Weldrake et al. 2003). Star formation in this galaxy began at least 10 Gyr ago (Clementini et al. 2003) and remains ongoing (Gallart et al. 1996; Hutchings et al. 1999). The galaxy is embedded in a large HI envelope (Weldrake et al. 2003). Previous spectroscopic studies, although incomplete, of supergiants (Venn et al. 2001), HII regions (Chandar et al. 2000), and red giant branch (RGB) stars (Tolstoy et al. 2001) found evidence of a gradient in [O/H] and measured an average [Fe/H] =  $-0.9$  dex with a spread of 1.5 dex. Most importantly, this galaxy has a large and widely distributed intermediate-age population (Battinelli et al. 2006) with a clear spread in metallicity (Cioni & Habing 2005). The C/M ratio has been estimated photometrically both from optical and near-IR criteria. This work provides the first comprehensive *spectroscopic* study of the AGB population of NGC 6822 dwarf irregular galaxy and its metallicity distribution.

We initiated a project to improve the C/M vs. [Fe/H] calibration using the large sample of intermediate-age stars in NGC 6822, for which we have a large database of near-IR photometry, low-resolution optical spectra useful to spectroscopically select C- and M-type AGB stars, as well as near-IR Ca II triplet spectroscopic observations used to indirectly measure [Fe/H]. Our preliminary results for the near-IR photometry were presented by Sibbons et al. (2010), and their full analysis is in preparation. This work analyses the near-IR optical spectra obtained with VIMOS multi-object spectrograph at the ESO VLT, and in a future article we will present the near-IR Ca II spectroscopic observations of AGB stars in NGC 6822.

## 2. Observations and data reduction

Our spectroscopic survey of M- and C-type AGB stars in the dwarf irregular galaxy NGC 6822 was made using the VIMOS imager and multi-object spectrograph (Le Fèvre et al. 2003) at

the ESO VLT UT3 telescope. The instrument is mounted on the Nasmyth B focus of UT3 Melipal and has four identical arms, each with a  $\sim 7' \times 8'$  FOV and a  $0''.205$  pixel size. The gap between the quadrants is  $\sim 2'$  and each quadrant is equipped with one EEV  $2k \times 4k$  CCD.

We first obtained mandatory R-band pre-imaging observations of seven fields in NGC 6822 in service mode. These pre-images were then used together with the wide field near-IR photometric catalogue obtained at UKIRT with WFCAM (Sibbons et al. 2010, Sibbons et al. 2011, in prep), to prepare the multi-object masks for spectroscopic follow-up observations in visitor mode, which comprised four masks (one per VIMOS quadrant) for each pointing.

We targeted seven fields, four centred on NGC 6822, and two outer fields. The central field had two different mask sets, each with 100-120 targets, while the other six fields had each one set of masks. In total, we targeted  $\sim 800$  stars in eight setups. The spectroscopic target selection was based on the UKIRT near-IR photometric data. All discussed magnitudes and colours in this study were corrected for foreground extinction according to the Schlegel et al. (1998) extinction map. All selected targets are brighter than 17.45 mag in  $K_0$  and have  $(J - K)_0 > 0.74$  mag, although redder stars were targeted preferentially. Cioni & Habing (2005) detected the RGB tip (TRGB) at  $K_s = 17.10 \pm 0.01$  mag, while Sibbons et al. (2010) report that it varies across the galaxy by  $\Delta K = 1.36$  mag, with an average value of  $K = 17.48 \pm 0.26$  mag. Davidge (2003) adopted a distance modulus of 23.49 mag based on the Cepheid and RGB tip measurements of Gallart et al. (1996), and measured the onset of the RGB tip in K band near  $K = 17$  mag. This is consistent with  $M_K^{\text{RGBT}} \sim -6.5$  mag. Gorski et al. (2011) identified the TRGB at  $K = 16.97 \pm 0.09$  mag.

Our observing log is presented in Table 1. In the second last column (slits), we report the number of slits for each pointing (sum of slits in four VIMOS quadrants), and in the last column (stars) we list the number of good quality recorded spectra (quality flags: 4, 5, or 6; see below) for each observed setup.

For our spectroscopic observations on August 22-24, 2009, we used the medium resolution grism (MR grism) and GG475 order sorting filter, which provides a spectral resolution  $R = 580$  ( $2.5 \text{ \AA}/\text{pix}$  dispersion) and a wavelength coverage from 500 to 1000 nm. The severe fringing in the red for the old VIMOS thinned and back-side illuminated, single-layer coated CCDs, used until May 2010 (Hammersley et al. 2010), meant that there was a significantly more restricted useful wavelength range of 500-780 nm in our spectra. Each setup was exposed for  $2 \times 20$  min.

We used the ESO VIMOS pipeline (version 2.5.2) to reduce the spectra. For each of the two observing nights, we took separate sets of bias frames and spectrophotometric standard-star observations. The reduction and extraction of the scientific exposures was performed in three steps with the following pipeline recipes. First we used the *vbias* recipe to create a master bias frame averaging the five bias frames. The *vmmoscalib* recipe was then used to obtain the wavelength calibration from the arc lamp spectra, trace the edges of the associated flat fields, and prepare all necessary tables for the scientific extraction.

We note that the flat-field exposures were only used to trace the slit edges and prepare the extraction tables. We decided not to apply a flat-field correction to our target spectra, as the flat fields were taken in the morning after the observing night. The different rotator angle and small differences in the positioning of the masks in the focal plane of the instrument may cause small shifts between the flat-field and science exposures, which could

**Table 1.** Observing log.

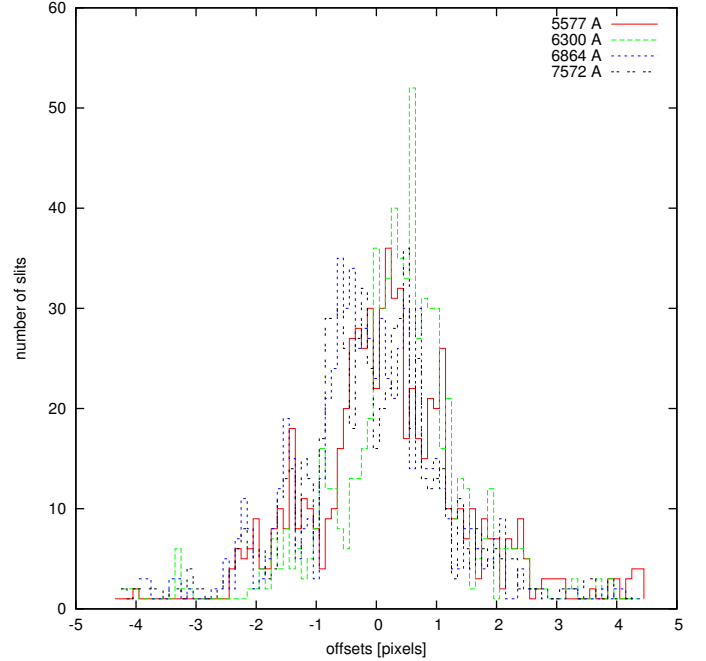
Night	Field	RA	DEC	Exposure [s]	Slits	Stars
		[hh:mm:ss]	[° : ' : '']			
22-23 Aug. 2009	CF1	19:44:56.75	-14:48:14.18	2 × 1200	119	57
	CF2	19:44:56.75	-14:48:14.18	2 × 1200	108	81
	NW1	19:44:20.77	-14:40:53.26	2 × 1200	108	47
	NE1	19:45:31.78	-14:40:52.64	2 × 1200	114	96
	SE1	19:45:33.78	-14:55:45.77	2 × 1200	123	115
23-24 Aug. 2009	SW1	19:44:19.78	-14:55:43.03	2 × 1200	101	62
	NE2	19:48:17.18	-14:24:45.94	2 × 1200	78	70
	SW2	19:42:09.78	-15:14:40.20	2 × 1200	70	18

then cause a decrease in the signal-to-noise ratio (S/N) after flat-fielding. We experimented with applying the flat-field correction but found that this neither improved nor decreased the spectrum S/N in the blue, while in the red part owing to fringing, spectra that were flat-fielded were actually noisier. We only find a difference in the third quadrant, where all exposures display some artificial drop in efficiency for certain wavelength ranges (most significantly around the sodium doublet, as most clearly seen in Fig. 5), which could not be fully corrected by applying a flat-field correction. This, however, did not affect our spectral classification.

The *vmossience* recipe was used to extract and calibrate the target spectra. This recipe applies the extraction mask obtained with *vmossalib*. The slit spectra are bias subtracted and remapped by eliminating the optical distortions. An additional wavelength calibration adjustment was made by fitting several strong sky emission lines. The final mean model accuracy of the wavelength calibration is about 0.15 pix, but the measurements of sky line offsets with respect to the expected wavelength sometimes have values of up to several pixels for individual spectra (Fig. 1).

We had acquired two scientific exposures for each observed field, which were aligned and stacked together. We adopted local sky subtraction and cosmic cleaning, and the optimal extraction method (Horne 1986) within the *vmossience* recipe. Finally, we applied the response curve, obtained from a spectrophotometric standard star observation. The reduction process of the standard star observations was analogous to the scientific ones. During the entire reduction process, we manually checked all spectra to verify spectral tracing, wavelength calibration, and object detection.

Unfortunately, the low resolution of our spectra and the very broad spectral features, prevented accurate measurements of the radial velocities of the targeted stars. On the basis of the Besançon model of our Galaxy (Robin et al. 2003), the expected median radial velocity and its standard deviation for the Milky Way foreground population of stars with  $15 < K < 17.5$  mag in the direction of NGC 6822 is  $1 \pm 44$  km/s. Owing to the overlap of this distribution with the radial velocity of NGC 6822 ( $-57$  km/s), which is based on HI data (Koribalski et al. 2004), and the radial velocities of the carbon stars obtained by Demers et al. (2006b) (between  $+10$  and  $-70$  km/s  $\pm 15$  km/s), combined with the uncertainty in our measured radial velocities, we decided not to rely on radial velocities to distinguish between the foreground dwarfs and NGC 6822 giant star members, but to instead use spectral features to distinguish the two populations. The classification of spectral types for all acquired spectra is described in Sect. 3.


**Fig. 1.** Distribution of offsets in pixels for four sky lines with respect to their expected wavelengths.

We used SExtractor (Bertin & Arnouts 1996) to derive R-band photometry from the pre-imaging, which was then calibrated using the NOMAD catalogue (Zacharias et al. 2005) based on about 200 stars in common with our observations. The calibration is presented in Fig. 2. We tested two fits to the data, a linear and a constant shift, which are presented in Eq. 1 and 2.

$$R_{\text{NOMAD}} = 1.08^{\pm 0.02} \times R_{\text{pre-imaging}} + 2.87^{\pm 0.27} \quad (\text{RMS} = 0.24), \quad (1)$$

$$R_{\text{NOMAD}} = R_{\text{pre-imaging}} + 4.03^{\pm 0.02} \quad (\text{RMS} = 0.25). \quad (2)$$

In obtaining the R-band photometry, we used the linear fit calibration (Eq. 1). All R-magnitudes were corrected for interstellar extinction according to Schlegel et al. (1998) using the NED extinction-law calculator. We note that the errors in the R-band photometry are larger than the errors of the IR-photometry because the NOMAD catalogue is a compilation of data from different sources.

### 3. Spectral classification

For each of our spectroscopic targets, we compiled near-IR photometric data based on the UKIRT photometry (Sibbons et al.

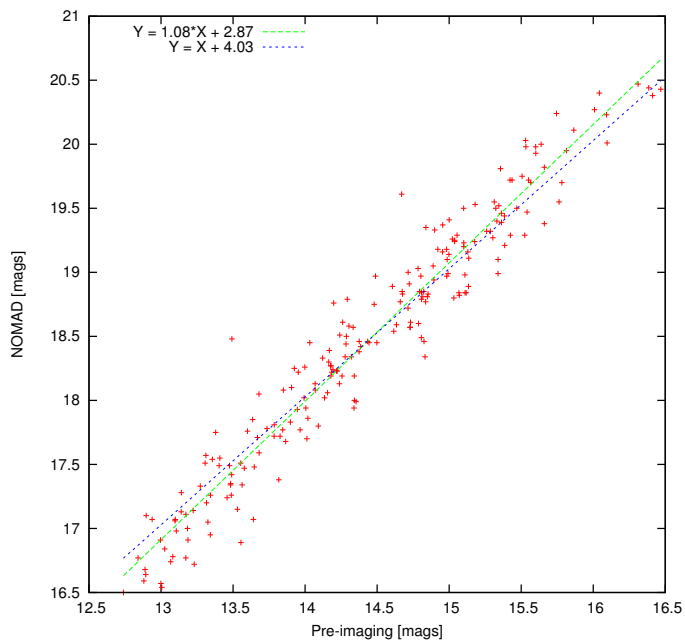


**Fig. 2.** R-band pre-imaging calibration. The lines are fits to the data indicated by the equations given within the figure.

2010) and complemented this with the spectral type based on reduced VIMOS spectra.

We determined the spectral class of each star mainly by visual comparing our spectra with those in the “Atlas of digital spectra of cool stars” (Turnshek et al. 1985). Where possible, we also compared our spectra with the spectral library of Jacoby et al. (1984). This spectral library is unfortunately less complete, in particular, there are not C-rich giants. To match the resolution of our spectra to that of the spectral atlas, and reduce the noise, we smoothed our spectra with a level 5 boxcar smoothing function using the *splot* IRAF task. Each spectrum was assigned one of the following quality flags, which are based primarily on the clarity of the spectral features, and not on the S/N: flag 2 for no detection; flag 3 for a poor quality spectrum, the star cannot be classified; flag 4, when we can determine whether the star is M- or C-type and eventually whether it is a giant or a foreground dwarf; flag 5 for very good quality spectra, the error in the spectral classification is within  $\pm$  one subtype; and flag 6 for an excellent quality and precise determination of the spectral class. The stars with lowest quality flags (2 or 3) were excluded from our final list. Fig. 3 shows typical examples of spectra with different quality flags. We indicate in this figure on top the primary spectral features that were used to assign a spectral type to M giants.

Typical M giants are characterized by TiO absorption bands, which are stronger for increasingly later spectral types. The telluric features O<sub>2</sub> and H<sub>2</sub>O are present in all spectra, because we did not apply a telluric correction, and are indicated at the bottom of the figure. The C-type giants can be quite easily distinguished as they have characteristic C<sub>2</sub> and CN molecular bands. The S-type stars display ZrO absorption features.

After we had performed an initial “by eye” spectral classification, we rescaled all spectra to an equal flux level and plotted them separately for each spectral sub-class to verify that indeed all spectra that had been assigned to that spectral sub-class had similar spectra. If an outlier was found, its spectral classification was repeated by comparing its spectrum with average spectra for different adjacent spectral classes. For each spectral subtype, we

compiled an average spectrum. Fig. 4 compares spectra of all M4 giants (green lines) with the spectrum from Jacoby et al. (1984) (dotted blue line), as well as the average M4 giant spectrum (red thick line). Similarly, Fig. 5 compares M0 dwarf spectra (green) with the average spectrum (red) and the M0 dwarf spectrum from Jacoby et al. (1984) (dotted blue line). We note that the molecular bands of the reference spectra from Jacoby et al. (1984) library are deeper, than those of average NGC 6822 spectra, most probably because of the higher metallicity of Milky Way stars. We tried to find information about the metallicities of the used reference stars in the Pastel database (Soubiran et al. 2010) but found data for only two reference giants, which both have solar metallicity. A comparison of synthetic spectra of different metallicities from the standard stellar library of Lejeune et al. (1997) reveals some differences in the depths of the main molecular bands and the shapes of the spectra. The stars of higher metallicity appear to have slightly later subtype than those of lower metallicity, at a given temperature and gravity. This means that our spectral classification of the M-type giants might be slightly underestimated, because of the lower average metallicity of NGC 6822 with respect to stars in the comparison spectral atlases (Turnshek et al. 1985; Jacoby et al. 1984), which are principally located in the solar neighbourhood.

The wide absorption feature around the Na I line in some of the M dwarf spectra (shown with green lines) in Fig. 5 is caused by flat field residuals. All spectra displaying these artifacts were acquired on the third quadrant CCD. We note that they are not real features. We note that all bands in the Jacoby et al. (1984) M0 V spectrum appear deeper than in our M0 V spectra. This is due to differences between the reference libraries. The M0 V spectral class of Jacoby et al. (1984) is indeed more consistent with the M1 V spectral class of Turnshek et al. (1985), which is our primary reference. Unfortunately, we could not find information about the metallicities of these reference stars in the literature.

Table 2 shows part of our final spectroscopic catalogue, the full version of which is available in electronic format. Column ID is the identifier of the stars, X and Y are the positions of the stars in the VIMOS pre-images, and column r is the distance from the centre of NGC 6822 (RA = 296.24059, DEC = -14.80343). The other columns list the  $R_0$ ,  $J_0$ ,  $H_0$ , and  $K_0$  magnitudes, the photometrically assigned spectral class (Sibbons et al. 2010), the classification based on our VIMOS spectra, and in the last column the quality flag of the spectra.

Different spectral subtypes are presented according to our classification in Fig. 6. The most similar dwarf and giant average spectra are plotted one over the other for comparison. It is easy to follow the change of some of the spectral features characteristic of M-type stars with increasing subtype. The strong sodium doublet (blended into a single line at our resolution) is the most typical feature of luminosity class V stars. With increasing subtype, it becomes weaker and dominated by the TiO band in the same wavelength range. For the later class dwarfs, we used the CaH molecular band at 6946Å, which deepens and widens the TiO bands in this region, to distinguish foreground dwarfs from giants. Another typical feature of the dwarf stars is the MgH band at 5211Å. The very late-type M dwarfs often display H $\alpha$  in emission, which may be evidence of magnetic activity. However, H $\alpha$  was not used as a criterion for distinguishing dwarfs from giants because it may also appear in emission in long-period variable stars (usually late-type AGB stars) in certain phases owing to shock fronts (Lançon & Wood 2000). In Fig. 7, we show individual example spectra for different types of C stars, easily

**Table 2.** Spectroscopic and photometric catalogue of stars observed in the direction towards NGC 6822. This is part of the full table, which is available in the electronic version of the paper.

ID	X [px]	Y [px]	RA [deg]	DEC [deg]	r [deg]	R [mag]	J [mag]	H [mag]	K [mag]	Sp. Cl. photometry	Sp. Cl. spectroscopy	Quality flag
94208	219.732	1679.789	296.349976	-14.828187	0.1121527	19.772	17.877	17.045	16.898	M	M1III	4
94979	330.734	1801.989	296.357117	-14.834526	0.1206048	19.510	17.528	16.720	16.515	Mca	M1III	4
96968	608.073	1462.465	296.337067	-14.850516	0.1073543	18.978	16.924	16.080	15.693	C	C5.5	5
97590	696.476	1751.644	296.354126	-14.855531	0.1249199	19.406	17.334	16.521	16.218	M	C5.5	5
99641	1001.033	2013.256	296.369537	-14.872893	0.1464667	20.196	17.025	15.971	15.317	C	C6.5	5
101911	1355.722	158.286	296.260742	-14.892557	0.09137722	20.645	17.952	17.153	16.985	M	M	4
77311	48.431	1099.388	296.316101	-14.679276	0.1453135	19.438	17.443	16.601	16.179	C	C6.5	5
79509	475.349	2029.313	296.371155	-14.703938	0.1641518	20.219	18.079	17.198	16.991	M	M1III	5
83906	1226.993	1566.500	296.343781	-14.746560	0.1178242	21.667	17.437	16.532	16.128	C	C5.5	5
85530	1462.654	1902.611	296.363739	-14.759742	0.1306686	23.344	16.528	15.565	14.986	C	C5.5	5
85885	1506.260	2089.456	296.374664	-14.762603	0.1401522	22.981	17.504	16.586	16.355	M	M4III	5
88539	1880.543	1058.628	296.313934	-14.783896	0.07590062	22.971	17.388	16.359	15.668	C	C5.5	4
77230	140.325	1975.243	296.193542	-14.678253	0.1337262	20.206	17.488	16.498	16.071	C	C5.5	5
78095	311.616	1734.144	296.179352	-14.688039	0.1306334	19.813	17.241	16.350	16.076	M	C5.5	5
78871	459.932	2256.131	296.210236	-14.696464	0.1111891	21.556	16.949	16.337	15.919	M	dM5e	5
79224	532.454	1875.599	296.187653	-14.700607	0.1156495	21.826	17.792	17.073	16.777	M	M6.5III	5
79511	589.745	1521.752	296.166718	-14.703956	0.1239035	20.233	17.724	16.890	16.697	M	M1III	4
80764	832.120	1828.010	296.184784	-14.717754	0.1022478	20.280	17.435	16.459	16.039	C	C5.5	5
81015	879.108	1219.159	296.148743	-14.720551	0.1237123	20.331	18.060	17.254	17.066	M	M1III	5
81290	923.831	1041.148	296.138214	-14.723130	0.130111	20.327	17.227	16.188	15.542	C	C6.5	5
82246	1076.064	1643.366	296.173828	-14.731837	0.09789109	20.061	17.335	16.543	16.299	M	M4III	6
83467	1267.180	2155.227	296.204193	-14.742633	0.07085879	18.691	15.048	14.173	13.874	M	M6III	6
83752	1310.298	1599.732	296.171265	-14.745203	0.09053338	20.500	18.020	17.228	16.970	M	C5.5	5
84020	1354.477	1830.278	296.185242	-14.747572	0.07863506	23.015	17.622	16.799	16.588	M	dM	5
85975	1628.458	2046.414	296.197662	-14.763362	0.0587216	20.414	17.175	16.255	15.536	C	C5.5	5
86798	1753.719	2238.658	296.208893	-14.769947	0.04610623	24.466	17.025	16.201	15.758	C	C6.5	5
88152	1934.647	2076.698	296.199615	-14.780900	0.04676038	20.389	18.414	17.421	17.201	C	M2III	5
88716	2021.618	2204.011	296.206879	-14.785284	0.03828439	19.733	18.082	17.209	17.074	M	C5.5	5
93532	99.508	1716.032	296.178833	-14.822721	0.06469996	20.139	17.330	16.475	16.210	M	SIII	5
93858	143.567	1738.309	296.180084	-14.825297	0.0643363	19.755	17.231	16.366	15.897	C	C5.5	6
94446	230.224	2278.535	296.212219	-14.830112	0.03894694	20.872	17.270	16.343	16.036	Cca	C8.2	5
94947	300.292	1631.935	296.173828	-14.834276	0.07354362	20.655	18.015	17.151	16.987	Mca	M1III	5
95293	347.628	1413.000	296.160797	-14.836968	0.08655488	20.626	18.027	17.370	17.092	Mca	dM3	6
73508 <sup>1</sup>	1469.541	1550.219	296.488861	-14.638191	0.2982319	20.405	17.496	16.557	15.974	C	C6.5 v	5
68214 <sup>1</sup>	636.571	1798.562	296.329102	-14.584000	0.2366088	19.231	17.611	16.957	16.665	M	M5 III e v	5
101802 <sup>2</sup>	1328.222	1947.256	296.365631	-14.891643	0.1530257	17.818	15.562	14.7120	14.318	C	M5III	6
100545 <sup>3</sup>	1120.211	656.699	296.116089	-14.881053	0.146717	20.608	17.310	16.2500	15.450	C	C5.5	6
86680 <sup>3</sup>	1308.239	1484.110	296.014832	-14.769041	0.2283621	18.537	17.050	15.8860	15.051	C	C8.2	5
111590 <sup>3</sup>	852.096	1197.049	295.993561	-14.990264	0.3097264	19.735	17.874	16.7020	15.840	C	C6.5	5

**Notes.** <sup>(1)</sup> LPV defined in Battinelli & Demers (2011). <sup>(2)</sup> IR spectrum from Groenewegen (2004) is available for this star. <sup>(3)</sup> C stars in common with the catalogue of Demers et al. (2006a).

distinguishable by means of the many CN and C<sub>2</sub> bands and an example of a rare S-type star clearly showing ZrO bands. We also plot the spectrum of a similar galactic S star from the atlas of Otto et al. (2011) over our example for comparison. Two figures showing separately the full sample of different subtypes giant and dwarf average spectra are available in the electronic version of the paper.

In total, we determined spectral types for 511 of the 546 spectra with quality flags of 4, 5, or 6 (Table 3). The majority turned out to be foreground dwarfs. This is in part because the colour criterion for the selection of AGB stars in NGC 6822 was on purpose quite relaxed ( $(J - K)_0 > 0.74$  mag) to allow the selection also of early-type M stars. In addition, if there was any remaining space in the masks after the primary targets were allocated to slits, then secondary targets, most of which were foreground dwarfs, were also targeted. Among the AGB stars belonging to NGC 6822, the majority are carbon-rich giants. Once again, this partly reflects the selection criteria, which were biased towards the AGB stars and in particular C-rich giants.

Battinelli et al. (2006) mapped the elliptical spheroid of NGC 6822 out to a semi-major axis distance of 36'. In Fig. 8, we show the spatial distribution of spectroscopically observed AGB stars in NGC 6822, as well as the Milky Way dwarfs, for which we have spectra of good quality. Essentially all giants identified by us as having either M-type or C-type AGB spectra are found within the ellipse, and the targets outside this region have been

**Table 3.** Statistics of the spectral classification for the different fields.

Field	All stars	M III	C III	S III	dwarfs	Unclass.
CF	138	55	64	4	8	7
NW1	47	7	10	0	28	2
NE1	96	22	25	1	39	9
SE1	115	24	36	2	48	5
SW1	62	14	16	2	29	1
NE2	70	0	0	0	62	8
SW2	18	1	0	0	14	3
All	546	123	151	9	228	35

systematically found to have spectral features typical of dwarf stars.

Battinelli & Demers (2011) published a catalogue of 63 long-period variable stars (LPVs) in NGC 6822. Cross-correlating our spectroscopic sample with their catalogue, we found two exact matches - a C giant (ID 73508), which is an irregular variable, and an M giant semi-regular variable (ID 68214) with a 149-day period. The latter shows H $\alpha$  line in emission. Another four variable sources were found within 10'' of our C and S stars, but without more information about the astrometric accuracy of the catalogue, we are unable to exclude that these are spurious matches and therefore do not report them

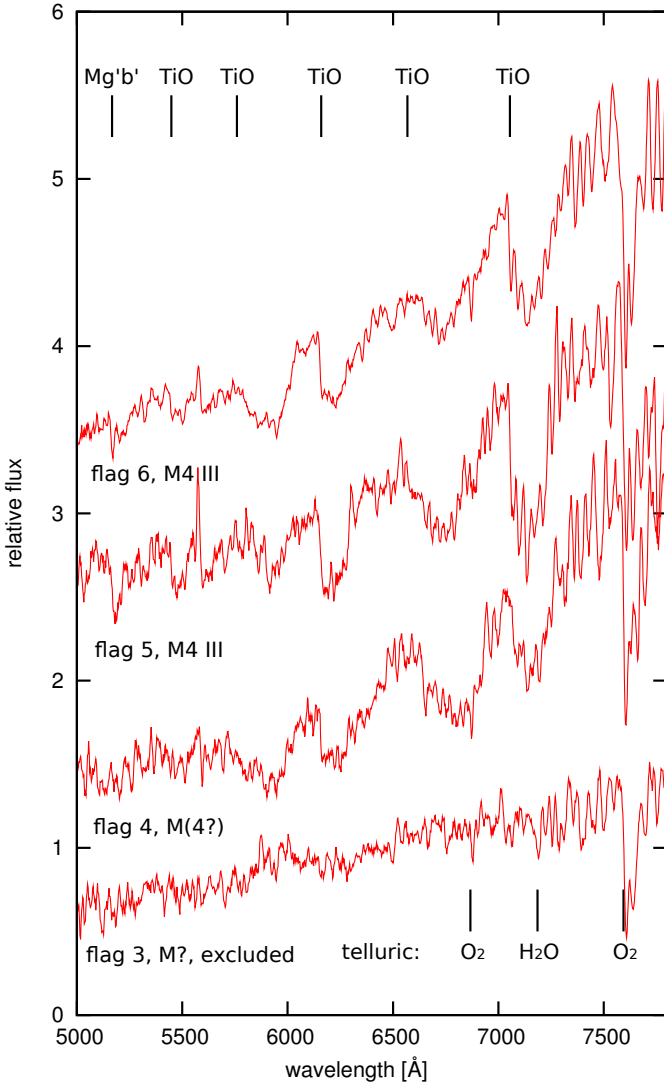


**Fig. 3.** Example of individual spectra with different quality flags. The spectra are rescaled, shifted along the y-axis by an arbitrary constant for presentation purpose, and smoothed with a level 5 boxcar function.

here. We also matched our catalogue with the 10 IR spectra obtained by Groenewegen et al. (2009) in NGC 6822. We found two exact matches with their targeted stars, one of which they actually observed (2MASS19452775-1453299) and we confirm that it is an M-type AGB star. Finally, we matched our catalogue with the catalogue of carbon stars (142 sources) obtained by Demers et al. (2006a). We found three exact matches, which were all confirmed as C-type stars based on our spectra. These have the following IDs in Demers et al. (2006a) catalogue: 1075, 1031, and 1026. Details about the stars in common with the cited catalogues are presented at the bottom of Table 2 marked with different indices. All stars that were matched based on coordinates with AGB samples of other authors, were also matched in spectral classification.

We emphasize the small overlap between our spectroscopic catalogue and the cited works. This might be partially explained by the limited choice of slit positions on the VIMOS masks. We also cross-correlated our full IR catalogue with these surveys and found that it contains 33 (from 63) sources from Battinelli & Demers (2011), 8 (from 10) sources from Groenewegen et al. (2009), and only 20 (from 142) sources from

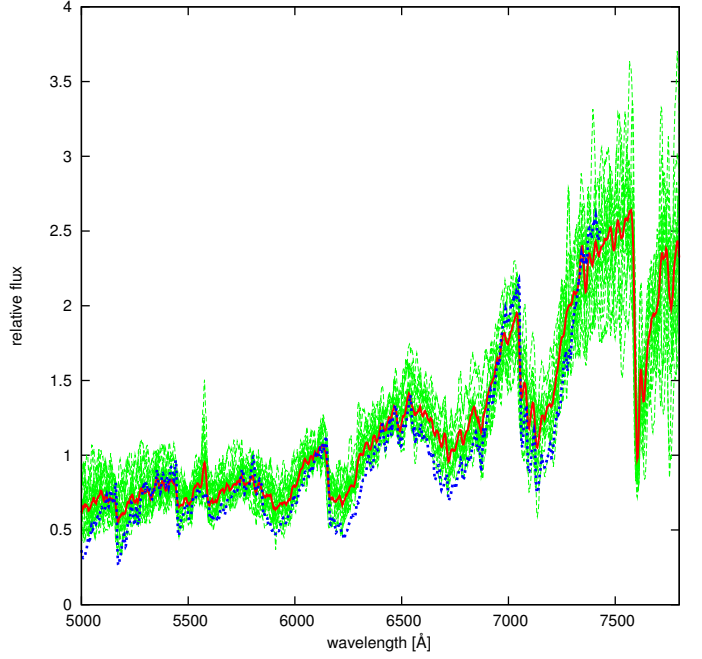


**Fig. 4.** All spectra classified as M4 III are rescaled and plotted together with green lines. An average M4 III spectrum is calculated and shown in red and a reference M4 III spectrum from the library of Jacoby et al. (1984) is drawn with a blue dotted line.

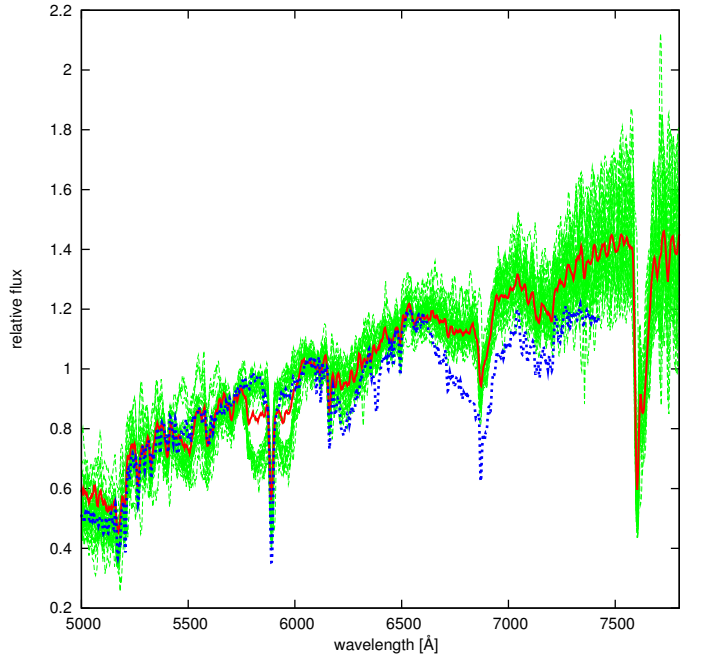


**Fig. 5.** Same as Fig. 4 but for M0 V spectral class.

Demers et al. (2006a). The astrometric differences are less than  $0.2''$  and the stars in common have similar  $J$  and  $K$  magnitudes. It is not trivial to answer where the biases in the full catalogue come from but this result might mean that our catalogue suffers from some incompleteness in either the outer regions of the galaxy, the redder part of the CMD, or both. All the stars in Demers et al. (2006a) have colours  $J - K > 1.5$  mag and are situated outside the central parts of NGC 6822. Other reasons could be the different criteria for selecting stellar sources or larger astrometry errors.

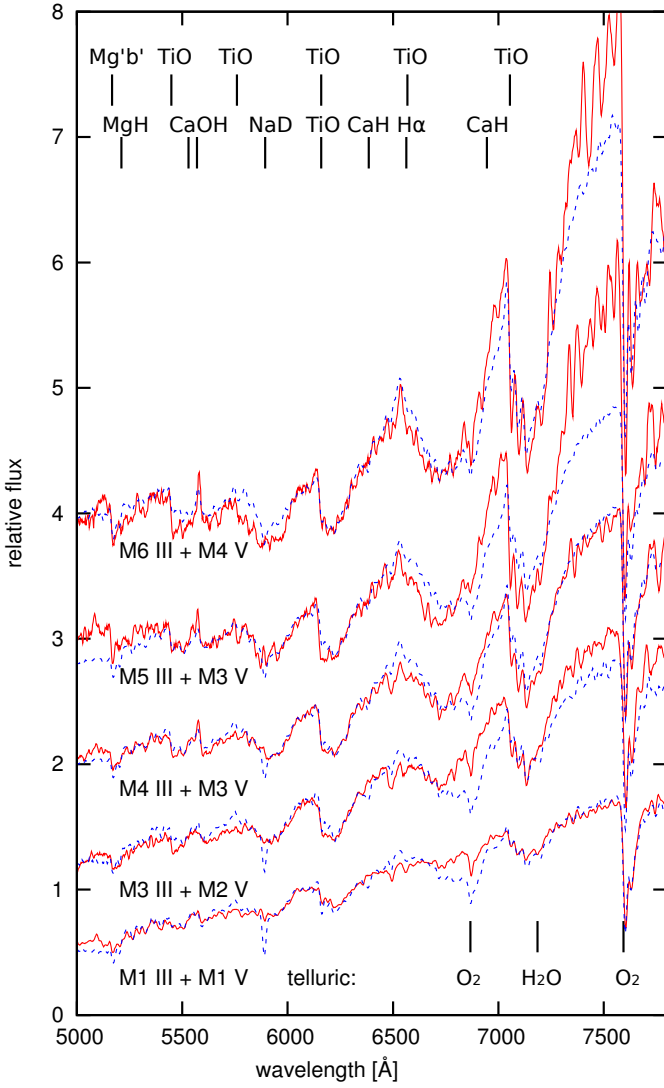


**Fig. 6.** Comparison between average dwarf and giant star spectra with similar spectral class. The similarities of the two types of spectra increase with increasing the spectral type. The spectra of giants are presented in red and the dwarfs with blue dotted lines. The positions of some of the most characteristic features (upper row for giants, second row for dwarfs) as well as some telluric bands (in the bottom) are shown with black lines. The spectra are shifted along the y-axis with an arbitrary constant for presentation purpose.

## 4. Results and discussion

### 4.1. Colour - magnitude and colour - colour diagrams

Fig. 9 shows the  $(J-K, K)$  colour-magnitude diagram (CMD) for all stars with good quality spectra. The diagram contains three distinct groups of objects - the two different types of AGB stars and the foreground population. They are depicted with different colour codes according to our spectral classification. We note that most of the M-type AGB stars have a colour index that is typically bluer than the  $(J-K)_0 = 1.2$  mag limit (Sibbons et al. 2010). The C-type stars, however, are dispersed across both sides of this limit. It is interesting that the bluer C-type stars, as well as the S-type stars are distributed preferably over the brighter end of the M star sequence. The foreground stars are distributed in a vertical sequence of  $(J-K)_0 \sim 0.8$  mag, that is easily

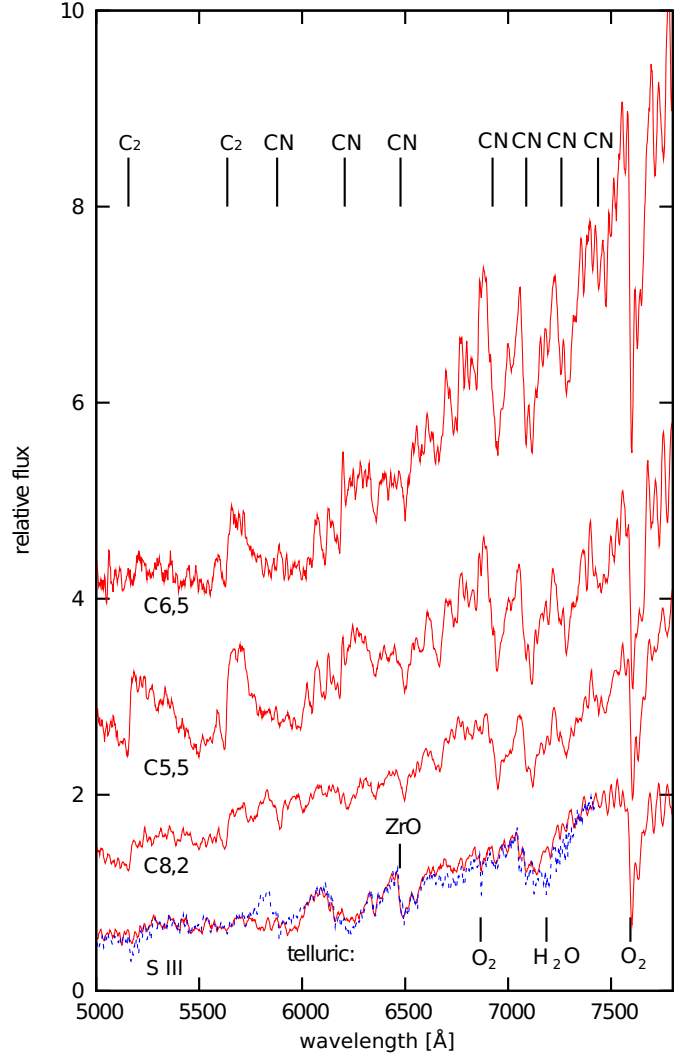


**Fig. 7.** Example spectra of individual stars of different C-types and one S-type plotted together. A spectrum of a similar star from the atlas of S stars (Otto et al. 2011) is overplotted with a blue dotted line for comparison. Positions of some of the most typical features are shown with black lines: C<sub>2</sub> and CN bands for the carbon stars and ZrO for the S-type stars. The spectra are shifted along the y-axis by an arbitrary constant for presentation purpose.

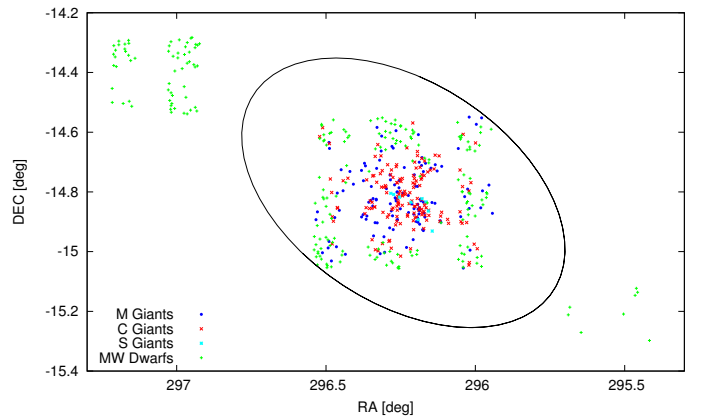


**Fig. 8.** Spatial distribution of all stars with acquired spectra of good quality. The outer 36' ellipse (Battinelli et al. 2006) is shown with solid black line. North is up and east is to the left.

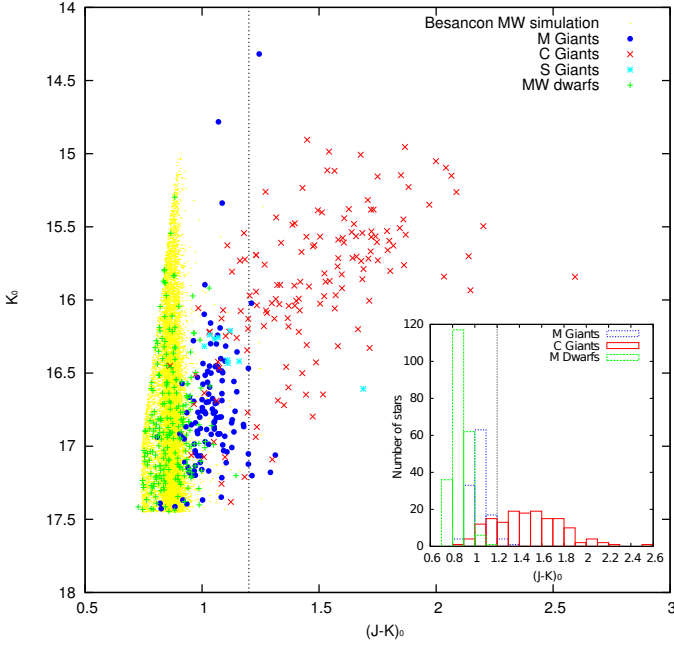


**Fig. 9.** CMD for all stars in the field of NGC 6822 with good quality spectra. The black dotted line shows the photometric selection criterion for differentiating between C- and M-type giants from Sibbons et al. (2010). The Milky Way dwarf sequence can be easily distinguished, even though it overlaps with the AGB sequence. The simulation of the foreground population obtained with the Besançon models is indicated by yellow dots. The smaller rectangle is a histogram of this CMD.

distinguishable but has a significant overlap with the AGB star distribution. This can be seen more easily in the histogram in Fig. 9. The histogram presents the number of classified stars vs. the  $(J - K)_0$  colour index in 0.1 magnitude bins. Most of the foreground Milky Way dwarfs have  $(J - K)_0$  colours between 0.7 and 1.0 mag, with maximum number of dwarfs being in the 0.8 – 0.9 mag bin. Most of the M giant stars are in the 1.0 – 1.1 mag bin and they strongly overlap with the dwarf sequence for the range  $(J - K)_0 \sim 0.9 - 1.0$  mag.

We used the Besançon model of the Milky Way (Robin et al. 2003) to simulate the foreground population. The model simulated about 11000 M- and K-type main sequence stars in total, within an area of 1.14 deg<sup>2</sup> centred on the centre of NGC 6822. The model parameters are chosen so that all simulated stars match the cuts of the full IR catalogue. The simulation agrees very well with the positions of the stars classified as dwarfs on the CMD. The simulated stars are shown with small yellow dots in Fig. 9. The Besançon model predicts roughly  $\sim 10000$  dwarfs per deg<sup>2</sup>, while in the full UKIRT catalogue the density of stars is  $\sim 7000$  stars per deg<sup>2</sup>, the large majority of which are dwarfs ( $\sim 6000$  per deg<sup>2</sup>).

Fig. 10 shows three two-colour diagrams. The  $(H - K, J - H)$  diagram (upper-right) is a powerful tool for separating the foreground Milky Way dwarfs and also allows a separation between the oxygen- and carbon-rich AGB stars (Aaronson & Mould 1985; Bessell & Brett 1988). In general AGB stars are expected to have  $(J - H)_0 > 0.73$  mag and all foreground dwarf stars should be bluer than this limit (Gullieuszik et al. 2008; Sibbons et al. 2010). Our spectra show that this is true for all spectroscopically observed stars with few exceptions. We find that the giants bluer than the  $(J - H)_0 = 0.73$  mag limit are mostly early M-type giants and only one is a C-type giant. There is one

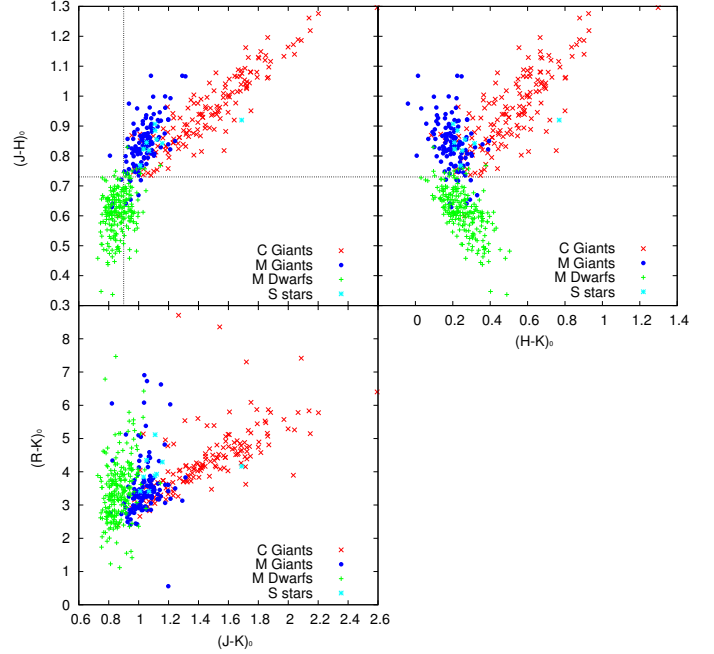


**Fig. 10.** Two-colour diagrams. Upper-left:  $(J - K, J - H)$  two-colour diagram. The two dotted lines show the AGB selection criteria:  $(J - H)_0 > 0.73$  mag and  $(J - K)_0 > 0.9$  mag; Upper-right:  $(H - K, J - H)$  two-colour diagram. The NGC 6822 carbon- and oxygen-rich AGB stars can be more clearly separated in this diagram; Bottom-left:  $(J - K, R - K)$  two-colour diagram.

dwarf star, which lies significantly redward of the colour limit at  $(J - H)_0 = 0.82$  mag. There is also a possibility that, owing to the high density of stars, few slits captured the light from neighbouring dwarf stars that were not the main target. We found this to be the case for one photometrically classified C-type star, which was targeted in two masks. In the spectrum from the first mask, we can clearly see a carbon-rich star and in the spectrum from the second mask, a foreground K dwarf. We excluded the spectra of four dwarf stars, which had been photometrically classified as carbon rich-stars, because of this effect. In the  $(J - K, J - H)$  two-colour diagram (upper-left), the C- and M-type giants are more intermixed but it shows our selection criteria for AGB stars. The horizontal line at  $(J - H)_0 = 0.73$  mag separates the foreground from NGC 6822 stars, and the vertical line at  $(J - K)_0 = 0.9$  mag indicates the blue limit for the AGB stars.

We also present the  $(J - K, R - K)$  two-colour diagram (bottom-left) in Fig. 10. It shows a clear separation between the different types of stars, which is however not as clean as for the IR photometry. This is mostly due to the larger R-band photometry errors and the probable variability of the targeted AGB stars (for which IR and R-band photometry were taken in different epochs), which would smear out their locations in the two-colour diagram. Otto et al. (2011) indicate that S-type stars are more clearly separated in this visible-IR two-colour diagram, which is also the case here. The colours of the Galactic S stars from Otto et al. (2011) are similar to the colours of S stars in NGC 6822.

#### 4.2. Photometric criteria for C vs. M giants selection based on the spectroscopic sample

On the basis of our spectroscopic sample, we derive new photometric selection criteria for distinguishing between different



**Table 4.** AGB stars selection from the photometric catalogue.

Criterion	M III	C III	S III	dwarfs
$(J - H)_0 > 0.72$	93%	99%	100%	9%
$(J - H)_0 > 0.73$	93%	99%	100%	6%
$(J - H)_0 > 0.74$	92%	98%	100%	5%
$(J - H)_0 > 0.75$	88%	96%	100%	3%
$(J - H)_0 > 0.73$ and $(J - K)_0 > 0.90$	92%	99%	100%	5%

types of AGB stars in NGC 6822 and foreground population. As already mentioned, the photometry is based on the near-IR catalogue of Sibbons et al. (2010). The selected photometric sample includes over 21000 stars found within a radius of 1 degree from the centre of NGC 6822, that are brighter than  $K_0 = 17.45$  mag in accordance with the value for the TRGB of NGC 6822 from Sibbons et al. (2010).

We find that the easiest way to differentiate between the AGB population of NGC 6822 and the foreground dwarfs is to use these two-colour diagrams. We tested several  $(J - H)_0$  cuts, and our results are summarized in Table 4. This table indicates the percentage of spectroscopically confirmed AGB stars that would be identified as AGB stars using a certain cut in  $(J - H)_0$ . We note that our spectroscopic sample contains almost no stars with the colours  $(J - H)_0 > 0.73$  mag and  $(J - K)_0 < 0.9$  mag (Fig. 10 upper-left diagram). These represent about 3% of the whole photometric sample, and because we are unable to determine their type, we exclude them. In this work, we use  $(J - H)_0 > 0.73$  mag and  $(J - K)_0 > 0.9$  mag to select AGB stars and  $(J - H)_0 < 0.73$  mag to select foreground stars. After applying these cuts, we found that our photometric sample includes about 2800 AGB candidates.

We propose two different approaches for distinguishing between carbon- and oxygen-rich AGB stars from the  $(J - K, K)$  CMD in order to estimate the C/M ratio. As we mentioned before, almost all S-type stars (8 of 9) and most of the C-type stars with colours  $(J - K)_0 < 1.2$  mag are brighter than  $K_0 = 16.45$  mag. We can also see that there are roughly equal numbers of M- and C-type stars in the region  $(J - K)_0 < 1.2$  mag and  $K_0 < 16.45$  mag according to our spectroscopic sample: 17 M-type and 18 C-type stars. Our first set of selection criteria (Fig. 11) is based on this result. We exclude all objects for which  $(J - K)_0 < 1.2$  mag and  $K_0 < 16.45$  mag. This permits us to remove the S-type stars as well as the region in the CMD where the C- and M-type stars strongly overlap but have a number ratio close to 1. We then simply divide the CMD into two parts: stars bluer than  $(J - K)_0 = 1.2$  mag, which we call M giants, and redder than  $(J - K)_0 = 1.2$ , which are C giants. If we adopt a distance modulus of 23.35 mag (weighted average obtained from Tables 4 and 5 in Gorski et al. (2011)), the absolute K magnitude of this limit will be  $M_K = -6.90$  mag.

The second approach is also based on cuts in the  $(J - K, K)$  CMD. We assume that all objects with  $(J - K)_0 < 1.2$  mag and  $K_0 > 2 \times (J - K)_0 + 14.05$  are M-type giants and objects with  $K_0 < 2 \times (J - K)_0 + 14.05$  and  $K_0 > -2 \times (J - K)_0 + 17.65$  are C-type giants (Fig. 12). This method provides the clearest possible separation between carbon- and oxygen-rich AGB stars but does not account for S-type stars. The excluded regions contain only 6% of the AGB candidates and the upper region might consist mostly of supergiants and foreground stars. In the fainter excluded region, we have three spectroscopically confirmed M giants and three C giants. Although we recognize the effect of small number statistics, there appears to be a large over-

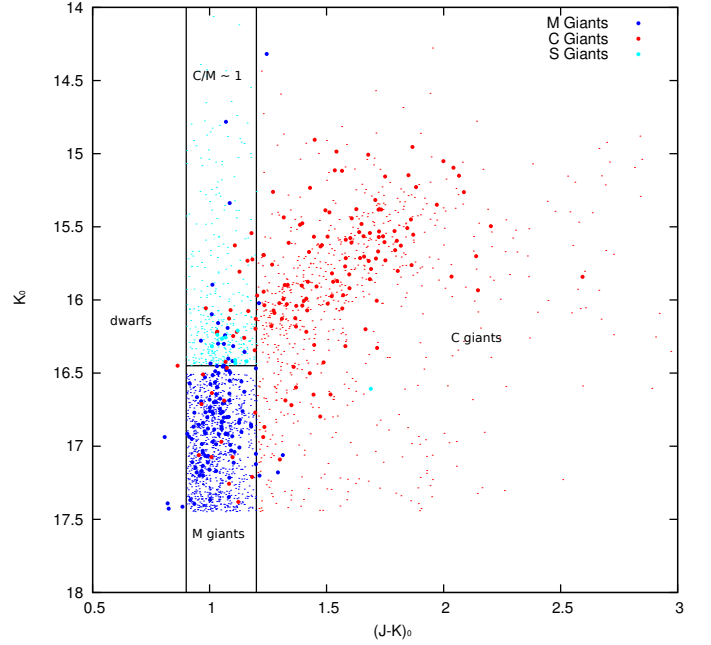


**Fig. 11.** First C- and M-type set of selection criteria. Most of the S-type stars and an equal number of C- and M-type stars are found in the region  $K_0 < 16.45$  mag,  $(J - K)_0 < 1.2$  mag. Excluding this region, our selection is based on a colour cut at  $(J - K)_0 = 1.2$  mag. The photometric sample is presented with dots and the spectroscopically confirmed stars with larger points.

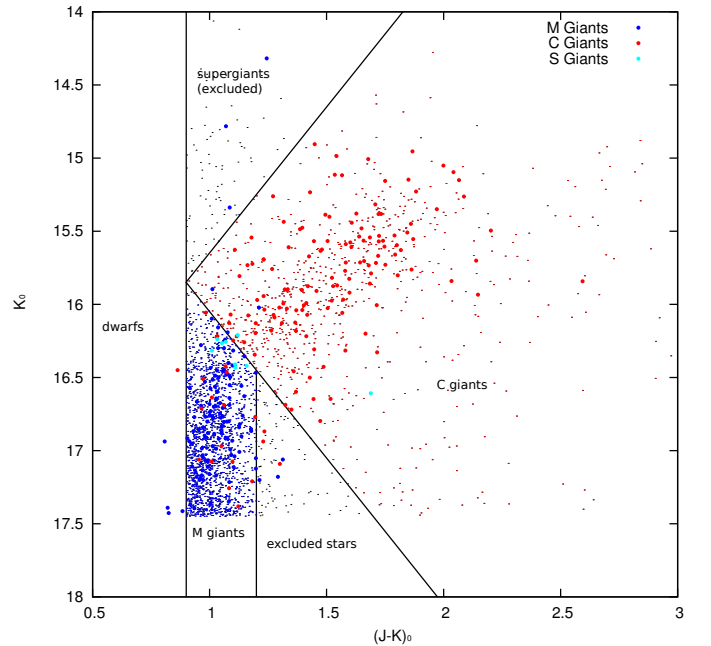


**Fig. 12.** Second C- and M-type set of selection criteria. The two excluded regions contain only 6% of the AGB candidates. The photometric sample is presented with dots and the spectroscopically confirmed stars with larger points.

lap between the C- and M-type stars in this region of the CMD. Adopting a distance modulus of 23.35 mag, and correcting for it, the selection criteria are all objects with  $(J - K)_0 < 1.2$  mag and  $M_K > 2 \times (J - K)_0 - 9.30$  are M-type giants and objects with  $M_K < 2 \times (J - K)_0 - 9.30$  and  $M_K > -2 \times (J - K)_0 - 5.70$  are C-type giants.

**Table 5.** Results of the C- and M-type star selection criteria.

I set criteria:	M-type sel.	C-type sel.	Excluded
Sp. M-type	74% + (14%)	4%	(14%)
Sp. C-type	9%	79% + (12%)	(12%)
Sp. S-type	0%	11%	89%
II set criteria:			
Sp. M-type	84%	2%	6%
Sp. C-type	11%	86%	2%
Sp. S-type	78%	22%	0%

**Table 6.** Expected contamination by different types of stars in the selection boxes.

I set criteria:	M-type selection	C-type selection
M-type cont.	79%	4%
C-type cont.	11%	95%
S-type cont.	0%	1%
dwarfs cont.	10%	0%
II set criteria:		
M-type cont.	75%	2%
C-type cont.	12%	97%
S-type cont.	5%	1%
dwarfs cont.	8%	0%

Tables 5 and 6 present the statistics of our selection criteria. In particular, Table 5 illustrates the effectiveness of both selection criteria. It lists the percentage of all spectroscopically classified stars for each spectroscopic class (e.g. M III, C III, S III) that coincides with the various photometric selection boxes (M-type selection, C-type selection, excluded). Table 6 instead shows the expected contamination of the M-type and C-type photometric selection boxes. This is estimated by assuming that the total number of spectroscopically confirmed stars in a given selection box (e.g. M-type selection or C-type selection box) is 100% and then computing the percentage of M-type, C-type, S-type, or dwarfs in that sample. We refer to this table when we discuss the overall C/M ratio in Sect. 4.3. The two selection criteria are good for the purpose of deriving the C/M ratio because some regions of the CMD, with reciprocal contamination, are excluded. They cannot be used to obtain the absolute number of C- and M-type stars in the galaxy.

#### 4.3. C/M ratio and metallicity distribution

Fig. 13 shows the number density of sources with good quality spectra. We counted the stars of a given spectral type in  $18 \times 18$  bins, where a single bin corresponds to  $2.0' \times 1.8'$  rectangle ( $36' \times 20'$  field). The source density in each map is smoothed with a boxcar function of  $width = 2$  prior to the construction of the greyscale images, where higher concentrations of sources are indicated with darker regions. From left to right, we show all stars, all AGB stars, and the foreground stars in the first row, and M-type AGB stars, C-type AGB stars, and the C/M ratio map in the second row. The size of the maps corresponds to the observed field within the outer ellipse of NGC 6822 according to Fig. 8 and is based on 271 AGB stars in total: 121 M- and 150 C-type giants. The number of individual stars is smaller than the number of obtained spectra because few stars were targeted in two of our masks. We can see from Fig. 13 that the AGB population is concentrated at the centre of the galaxy. However the large C/M ratio in the central parts (which varies between 1 and 2) is due

to underestimating the number of M stars with respect to the C stars and it is possible that the small C/M ratio in the outer parts is due to small number statistics. These maps reflect the biases in the spectroscopic sample (C stars were targeted preferentially) and cannot be used to derive the metallicity distribution within the galaxy.

To investigate the C/M ratio and metallicity distribution within NGC 6822, we use the complete near-IR photometric catalogue. Here we apply the second set of photometric selection criteria (discussed in the previous section) to distinguish between carbon- and oxygen-rich AGB stars. We obtain very similar results when the first set of criteria is used. The results are presented in Fig. 14, which is almost identical to Fig. 13 but the stars are binned in  $36 \times 36$  bins, of  $1' \times 0.9'$  each. The map is based on 1753 AGB stars in total, 970 and 783 photometrically classified M- and C-type stars, respectively. We would expect the foreground density map to be flat but we can see some overdensity of stars at the centre coinciding with the galaxy. This means that we underestimate the number of AGB stars, which are most probably M-type giants. This overdensity is quite small, only  $1.3 \sigma$  over the foreground fluctuations and has no significant effect on our C/M ratio estimate.

The overall C/M ratio is 0.8 according to the number of stars in the selection boxes. However, if we take into account the expected contaminations in the selection boxes from Table 6, i.e. the number of M giants to be 75% of the number of stars in the M-type selection box plus 2% of the number of stars in the C-type selection box plus 4% from the dwarfs selection and the number of C giants to be 97% of the C-type selection plus 12% of the M-type selection, we calculate a C/M ratio  $\sim 1.05$ . This value is in excellent agreement with C/M ratio of 1.0 obtained by Letarte et al. (2002).

We see a similar trend in the C/M ratio distribution across the galaxy as described by Cioni & Habing (2005). The galaxy centre has a relatively small C/M ratio that increases when moving outwards. The maximum of the C/M ratio follows a broken ellipse around the galactic centre and then starts to decrease with increasing radii. This decrease in the C/M ratio towards the outer regions may be real or due to small number of statistics. A bar-like structure traced by younger stars in Gouliermis et al. (2010) cannot be distinguished in the C/M ratio distribution. The area investigated by Karamelas et al. (2009) corresponds to the field of Fig. 14. Beyond that, the density of stars is too low and it is difficult to estimate the C/M ratio. We discuss the stellar density in the outermost regions of our photometric catalogue in Sect. 4.5.

The variation in the C/M ratio across the face of the galaxy can be explained by a variation in the metallicity. A higher C/M ratio relates to a lower metallicity. This relation is well-studied in previous works of Cioni & Habing (2003, 2005) for the SMC, LMC, M 33, and this galaxy, and calibrations between C/M and [Fe/H] were presented in Groenewegen (2004), Battinelli & Demers (2005), and Cioni (2009). The physical reasons for this correlation are explained by Scalo & Miller (1981) and Iben & Renzini (1983): (i) O-rich AGB stars of lower metallicity turn more easily into C-rich stars; (ii) evolutionary tracks for lower metallicities correspond to higher temperatures; (iii) in very low metallicity environments, post-horizontal branch stars may fail to become AGB stars.

In our study of NGC 6822, the C/M ratio varies between 0.2 and 1.8 according to Fig. 14 and this corresponds to a metallicity variation of  $\Delta[\text{Fe}/\text{H}] \sim 0.4$  dex (between  $-0.9$  dex and

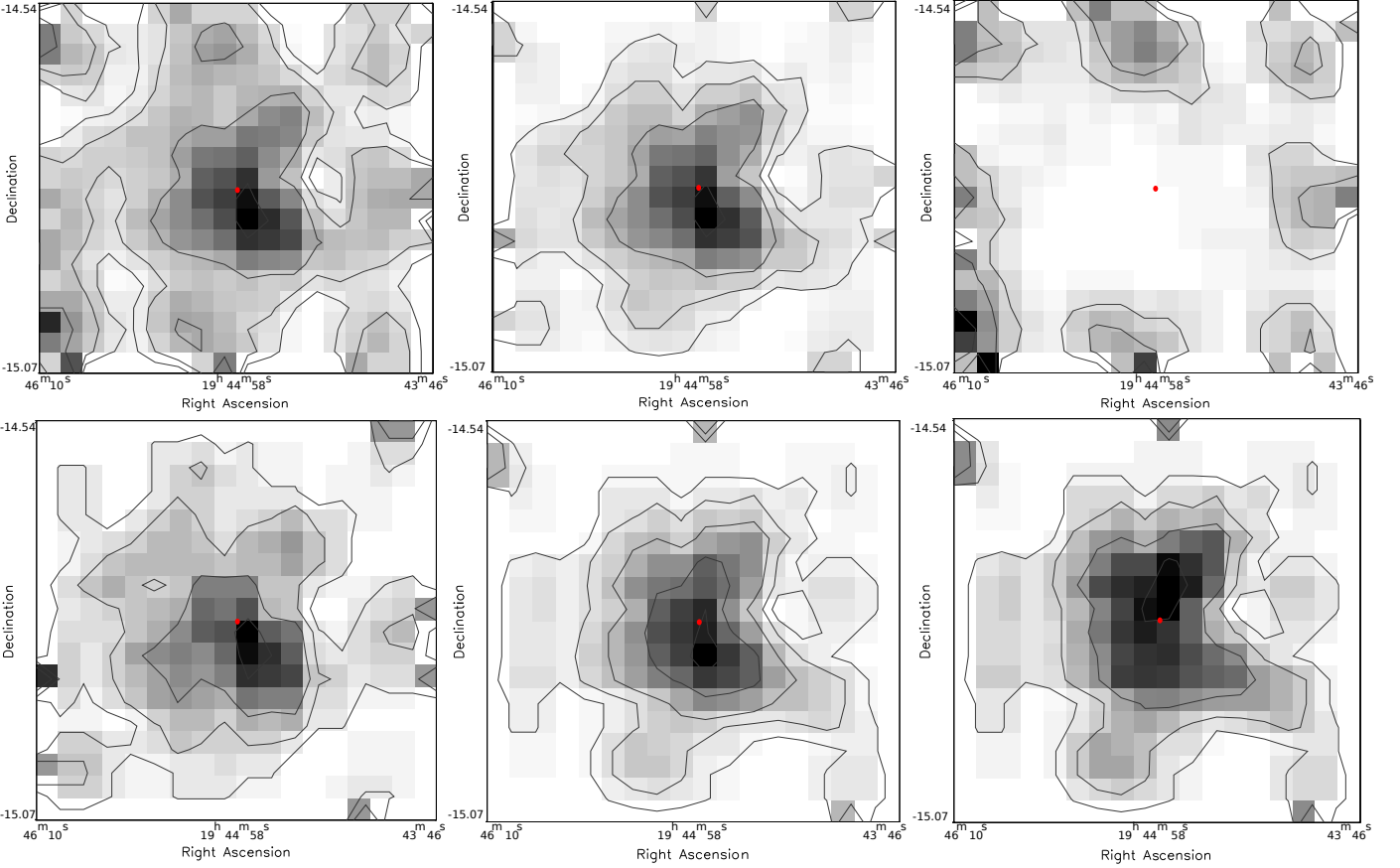


**Fig. 13.** Logarithmic and smoothed density distributions of all stars with good quality spectra. The maps are in  $18 \times 18$  bins  $2.0' \times 1.8'$  each as follows; top: all stars, all AGB stars, and all dwarf stars (contours are for 0.5, 1, 2, 5 density levels); bottom: M-type AGB stars, C-type AGB stars (contours are for 0.2, 0.5, 1, 2, 3 density levels), and C/M ratio map (contours are for ratios 0.2, 0.5, 1, 2). Darker regions correspond to higher density. The centre of the galaxy is indicated with a small red dot. North is up and east is to the left.

$-1.3$  dex) with an average  $[\text{Fe}/\text{H}] \sim -1.2$  dex using the calibration proposed by Groenewegen (2004)

$$[\text{Fe}/\text{H}] = -0.42 \times \log(C/M) - 1.23. \quad (3)$$

Another calibration proposed by Battinelli & Demers (2005) is

$$[\text{Fe}/\text{H}] = -0.59 \times \log(C/M) - 1.32. \quad (4)$$

Using this we obtain an average value of  $[\text{Fe}/\text{H}] \sim -1.3$  dex with a spread of between  $-0.9$  dex and  $-1.5$  dex. A revision of Eq. 4 is presented in Cioni (2009), who propose the alternative relation

$$[\text{Fe}/\text{H}] = -0.47 \times \log(C/M) - 1.39. \quad (5)$$

For NGC 6822, we get an average value of the  $[\text{Fe}/\text{H}]$  index  $\sim -1.3$  dex with a spread of between  $-1.1$  dex and  $-1.5$  dex. If we adopt  $C/M$  ratio  $\sim 1.05$ , the obtained metallicity values are slightly lower, but still very similar to the  $[\text{Fe}/\text{H}]$  values discussed here. The metallicity estimates are in good agreement with the results of Tolstoy et al. (2001) and Davidge (2003). The former study found an average  $[\text{Fe}/\text{H}] = -1.0 \pm 0.5$  dex with a spread of between  $-0.5$  and  $-2.0$  dex based on Ca II spectroscopic measurements of 23 RGB stars, while the latter derived  $[\text{Fe}/\text{H}] = -1.0 \pm 0.3$  dex from the slope of the RGB. A measurement of the Ca II triplet absorption lines in a statistically significant number of AGB stars in NGC 6822 is the subject of a subsequent paper by our team to provide an independent estimate of the metallicity index.

#### 4.4. C/M ratio and possible age variations

Feast et al. (2010) suggested that radial trends of the C/M ratio across the galaxy might also be explained by age rather than metallicity variations. We test this possibility by fitting isochrones from the Padova library (Marigo et al. 2008; Girardi et al. 2010). The comparison with isochrones shows that the AGB stars are older than 0.8 Gyr but an upper age limit is difficult to establish because the isochrones become uncertain for ages  $> 2.0$  Gyr in this region of the CMD. We compare different regions of high and low C/M ratios in the galaxy with isochrones for ages 1.0 and 1.5 Gyr and metallicities between  $-0.7$  and  $-1.3$  dex. We see that regions with larger ratios have slightly tighter fits by isochrones of age 1.5 Gyr, thus are a bit older than the regions with relatively smaller ratios, which are more consistent with isochrones of age 1.0 Gyr (Fig. 15). The selected regions are marked on the C/M ratio map in Fig. 14: blue for smaller and red for larger ratios. We note, however, that there are a number of uncertainties such as whether there is a significant intrinsic reddening, and any uncertainty in both the distance modulus and the theoretical models themselves, that could bias the conclusions.

In accordance with this line of thought, the slight shift in the peak of the M star distribution with respect to the C stars is unsurprising and probably means that the photometric selection criteria select M stars that are younger than the bulk of C stars. While the densest concentration of C stars is located at the cen-

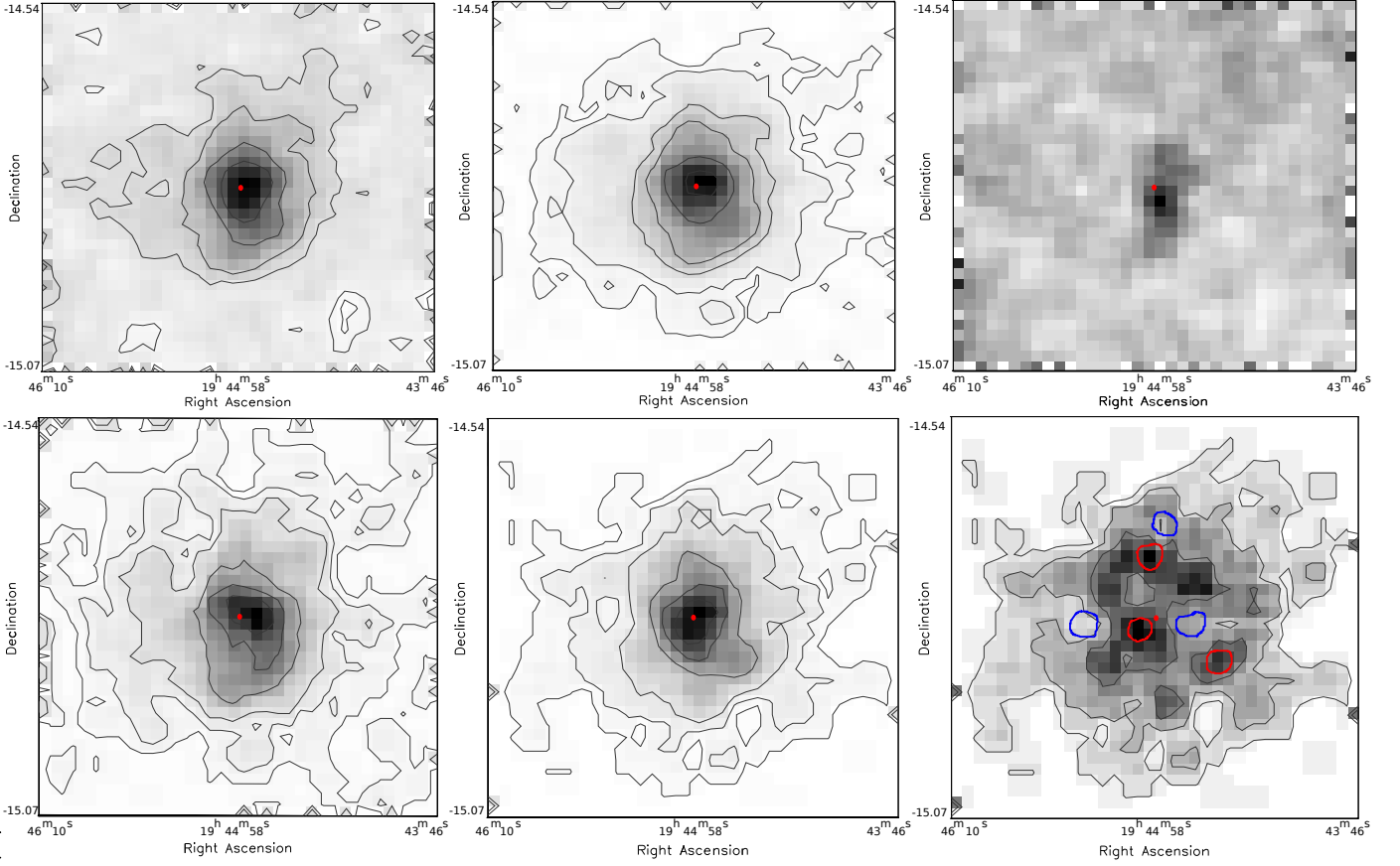


**Fig. 14.** Logarithmic and smoothed density distributions of the stars from the near-IR catalogue. The maps are in  $36 \times 36$  bins  $1.0' \times 0.9'$  each as follows; top: all stars, all AGB stars, and all dwarf stars (contours are for 0.5, 1, 3, 5, 10, 15 density levels); bottom: M-type AGB stars, C-type AGB stars (contours are for 0.2, 0.5, 1, 3, 5, 7 density levels), and C/M ratio map (contours are for ratios 0.2, 0.5, 1). Darker regions correspond to higher density. The centre of the galaxy is indicated with a small red dot. The blue circles indicate low and the red circles high C/M regions that are further discussed in Sects. 4.4 and Fig. 15. North is up and east is to the left.

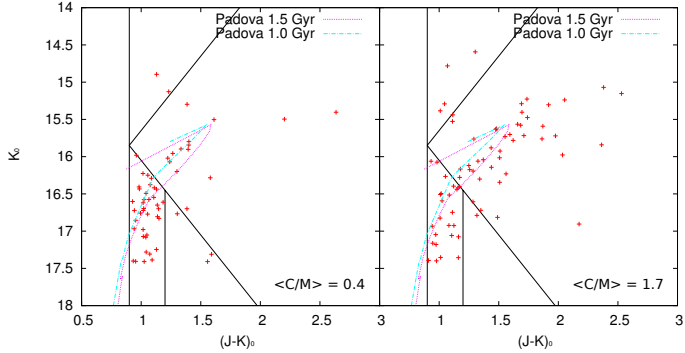


**Fig. 15.** Stars from three regions of high and low C/M ratios are plotted and compared with isochrones for  $[\text{Fe}/\text{H}] = -1.0$  dex and ages 1.0 and 1.5 Gyr. The selected regions are indicated in Fig. 14. It seems that larger ratios refer to slightly older ages.

tre of NGC 6822, the M star distribution peaks about  $1'$  west of it, centred on a bright UV-emission region of recent star formation detected by GALEX (region 26, defined in Efremova et al. (2011)).

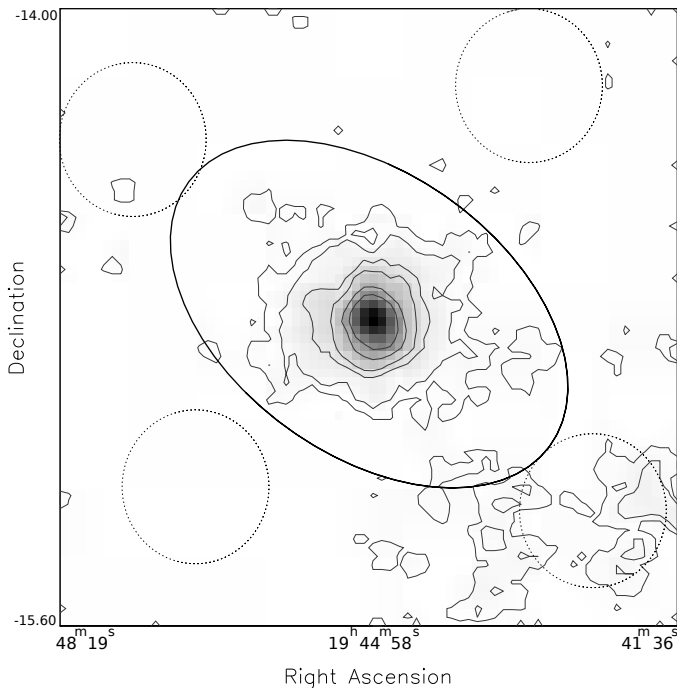
#### 4.5. Structure of NGC 6822

The near-IR catalogue covers a region of roughly one degree from the centre of NGC 6822. This allows us to investigate the stellar density of probable galaxy members to this extent. Using the second set of selection criteria, we found that 93% of the photometrically classified C giants and only 64% of the M giants are within the outer ellipse of Battinelli & Demers (2005). We studied the stellar density and the interstellar extinction (using the Schlegel et al. (1998) extinction maps) towards four fields (indicated in Fig. 16 and referred to as NW, SW, NE and SE in Table 7) outside the Battinelli ellipse. We note that a larger number of possible galaxy members extends to the south-west at least one degree from the NGC 6822 centre. The overall stellar density in the south-west field is indeed a little higher than the average foreground density, and the extinction is the same as towards the centre of the galaxy,  $E(B - V) = 0.24$  mag.

We see that there is some variation in the extinction between these four fields, which is lower in the north-west and north-east fields, but that this difference corresponds to a  $\Delta E(J - H) = 0.02$  mag correction to the  $J - H$  colour index, which is the principal means of AGB star selection. Hence, we can assume that the IR extinction in the field of the entire near-IR catalogue is rather constant. In the M III column of Table 7, we list the number of M-type AGB candidates per field assuming a constant  $E(B - V) = 0.24$  mag in all fields and in brackets we list

**Table 7.** Stellar density in four outer fields around NGC 6822, considering only the AGB population ( $K < 17.45$  mag).

Field	RA [deg]	Dec [deg]	Radius [deg]	M III count	C III count	Dwarfs count	Fraction of AGB AGB/all	Total st. density [stars p. sq. arcmin]	$E(B - V)$ [mag]
NW	295.794	-14.198	0.2	25 (48)	0	892	0.03	2.028	0.172
SE	296.702	-15.240	0.2	13 (13)	3	848	0.02	1.911	0.226
NE	296.873	-14.338	0.2	31 (43)	2	746	0.04	1.723	0.187
SW	295.620	-15.302	0.2	130 (130)	11	864	0.14	2.223	0.241


**Fig. 16.** Smoothed and logarithmic density map of all AGB candidates within the entire field of the IR catalogue. We see a rather significant excess of stars south-west of the centre of the galaxy. The map consists of  $72 \times 72$  bins,  $1.4 \times 1.3$  arcmin each. Contours are for 0.5, 1, 3, 5, 10, 15 density levels. The Battinelli & Demers (2005) ellipse and the four discussed outer fields are sketched along. North is up and east is to the left.

the number of M-type AGB candidates that we would have if we adopt the appropriate extinction value from the last column of Table 7. The extinction correction does not lead to any new C-type AGB candidates in the sample but we note that a small correction to the  $J - H$  limit could have a significant impact on the number of M-type AGB stars and foreground stars. About 10% of the photometrically recognized galaxy members may actually be foreground dwarfs according to our selection criteria. A logarithmic and smoothed density map of all AGB candidates within the field of the near-IR catalogue is presented in Fig. 16. The isodensity contours that we obtain are very similar to the map presented in Letarte et al. (2002, see their Fig. 9).

We can also consider the full photometric catalogue, which, although not complete, extends to a faintness level of  $K_0 = 19$  mag. We adopt  $(J - H)_0 > 0.73$  mag to select RGB and AGB candidates (a  $J - K$  limit is not adopted because of the expected slope in the RGB) and investigate the stellar densities within the same four outer fields. We again see higher density of possible members of NGC 6822 towards the south-west, although less pronounced because of the unavoidable higher contamination of foreground stars in the selected sample.

Hence, this excess of stars seems to be real but a spectroscopic confirmation of their membership to the galaxy is required.

## 5. Conclusion

We have presented spectroscopic observations of about 800 stars in the field of the NGC 6822 dwarf galaxy, 511 of which are of good enough quality to permit a reliable spectral classification. The observed stars have been classified as M, C, and S spectral types or foreground dwarfs according to their typical spectral features. We have presented the largest spectroscopic catalogue to date of carbon and oxygen rich AGB stars in NGC 6822. Their distribution in colour-magnitude and colour-colour diagrams was discussed, and we proposed and quantified new photometric selection criteria between the different types of stars. Foreground stars tend to have colours  $(J - H)_0 < 0.73$  mag and follow a vertical sequence with a peak at  $(J - K)_0 \sim 0.8$  mag on the  $(J - K)_0$  vs.  $K_0$  CMD. This was also confirmed by the Besançon Milky Way model (Robin et al. 2003). We found, however, that this model overpredicts the stellar density in the direction of NGC 6822. We also conclude that a small variation in the dwarfs vs. AGB selection criteria may have a significant impact on the number of AGB stars with respect to the foreground.

Our selection of C- and M-types giants was based on selection boxes in the  $(J - K)_0$  vs.  $K_0$  CMD. These criteria were applied to the near-IR photometric catalogue of Sibbons et al. (2010) and the surface distribution of the C/M ratio was discussed. We used the C/M ratio as a metallicity indicator and found that the galaxy has an average metallicity index  $[Fe/H] \sim -1.2 \div -1.3$  dex with a spread of  $\Delta[Fe/H] \sim 0.4 \div 0.6$  dex according to the different C/M vs. metallicity calibrations. Regions of larger C/M ratio (lower metallicity) are preferably distributed across a broken ellipse around the centre, which itself has a smaller ratio (higher metallicity). We also discussed whether the trends in the C/M ratio are driven by age rather than metallicity variations. A comparison with isochrones suggests that regions of higher C/M ratio are slightly older than the regions of lower C/M ratio.

The wide area of the IR catalogue allows us to investigate the field of NGC 6822 out to one degree from its centre. We detected a significant overdensity of possible AGB stars south-west of the galaxy centre, but confirmation of their membership would require spectroscopic data.

*Acknowledgements.* The spectroscopic observations were acquired together with L. Sibbons, whose assistance is gratefully acknowledged. We are indebted to Carlo Izzo for his dedicated support and development of the VIMOS pipeline, including comprehensive documentation and helpful suggestions on data reduction. We thank Antoniya Valcheva for useful comments and notes on the paper. We gratefully acknowledge funding for this project by the ESO DGDF grant. The project was partially funded by the Bulgarian NSF (contract No DDUV02/40/2010). This research has made use of the NASA/IPAC Extragalactic Database (NED) which is operated by the Jet Propulsion Laboratory, California Institute of Technology, under contract with the National Aeronautics and Space Administration. We thank the anonymous

referee and the editor Ralf Napiwotzki, whose comments helped to improve the paper.

## References

- Aaronson, M. & Mould, J. 1985, *ApJ*, 290, 191  
 Battinelli, P. & Demers, S. 2004, *A&A*, 416, 111  
 Battinelli, P. & Demers, S. 2005, *A&A*, 434, 657  
 Battinelli, P. & Demers, S. 2011, *A&A*, 525, 69  
 Battinelli, P., Demers, S., & Kunkel, W. E. 2006, *A&A*, 451, 99  
 Bertin, E. & Arnouts, S. 1996, *A&AS*, 117, 393  
 Bessell, M. S. & Brett, J. M. 1988, *PASP*, 100, 1134  
 Cassisi, S., Castellani, V., Degl'Innocenti, S., Piotto, G., & Salaris, M. 2001, *A&A*, 366, 578  
 Chandar, R., Bianchi, L., & Ford, H. C. 2000, *AJ*, 120, 3088  
 Cioni, M.-R. L. 2009, *A&A*, 506, 1137  
 Cioni, M.-R. L. & Habing, H. J. 2003, *A&A*, 402, 133  
 Cioni, M.-R. L. & Habing, H. J. 2005, *A&A*, 429, 837  
 Cioni, M.-R. L., Irwin, M., Ferguson, A. M. N., et al. 2008, *A&A*, 487, 131  
 Cioni, M.-R. L., Irwin, M., Ferguson, A. M. N., et al. 2009, *A&A*, 500, 1025  
 Clementini, G., Held, E. V., Baldacci, L., & Rizzi, L. 2003, *ApJ*, 588, 85  
 Davidge, T. J. 2003, *PASP*, 115, 635  
 Demers, S., Battinelli, P., & Artigau, E. 2006a, *A&A*, 456, 905  
 Demers, S., Battinelli, P., & Kunkel, W. 2006b, *ApJ*, 636, 85  
 Efremova, B. V. and Bianchi, L., Thilker, D. A., Neill, J. D., et al. 2011, *ApJ*, 730, 88  
 Feast, M. W., Abedigamba, O. P., & Whitelock, P. A. 2010, *MNRAS*, 408, 76  
 Gallart, C., Aparicio, A., Bertelli, G., & Chiosi, C. 1996, *AJ*, 112, 1950  
 Gallart, C., Aparicio, A., & Vilchez, J. M. 1996, *AJ*, 112, 1928  
 Gallart, C., Zoccali, M., & Aparicio, A. 2005, *ARA&A*, 43, 387  
 Girardi, L. & Marigo, P. 2007, *A&A*, 462, 237  
 Girardi, L., Williams, B. F., Gilbert, K. M., et al. 2010, *ApJ*, 724, 1030  
 Gorski, M., Pietrzynski, G., & Gieren, W. 2011, *AJ*, 141, 194  
 Gouliermis, D. A., Schmeja, S., Klessen, R. S., de Blok, W. J. G., & Walter, F. 2010, *ApJ*, 725, 1717  
 Groenewegen, M. A. T. 2004, arXiv:astro-ph/0407282, invited review at the conference: "Planetary Nebulae beyond the Milky Way"  
 Groenewegen, M. A. T., Lançon, A., & Marescaux, M. 2009, *A&A*, 504, 1031  
 Gullieuszik, M., Held, E. V., Rizzi, L., Girardi, L., & Marigo, P. and Momany, Y. 2008, *MNRAS*, 388, 1185  
 Hammersley, P., Christensen, L., Dekker, H., et al. 2010, *The Messenger*, 142, 8  
 Horne, K. 1986, *PASP*, 98, 609  
 Hutchings, J. B., Cavanagh, B., & Bianchi, L. 1999, *PASP*, 111, 559  
 Iben, I. J. & Renzini, A. 1983, *ARA&A*, 21, 271  
 Jacoby, G. H., Hunter, D. A., & Christian, C. A. 1984, *ApJS*, 56, 257  
 Karamelas, A., Daperoglas, A., Kontizas, E., & et al., L. 2009, *A&A*, 497, 703  
 Koribalski, B. S., Staveley-Smith, L., Kilborn, V. A., et al. 2004, *AJ*, 128, 16  
 Lançon, A. & Wood, P. R. 2000, *A&A*, 146, 217  
 Le Fèvre, O., Saisse, M., Mancini, D., et al. 2003, in Presented at the Society of Photo-Optical Instrumentation Engineers (SPIE) Conference, Vol. 4841, Society of Photo-Optical Instrumentation Engineers (SPIE) Conference Series, ed. M. Iye & A. F. M. Moorwood, 1670–1681  
 Lejeune, T., Cuisinier, F., & Buser, R. 1997, *A&AS*, 125, 229  
 Letarte, B., Demers, S., Battinelli, P., & Kunkel, W. E. 2002, *AJ*, 123, 832  
 Lyubenova, M., Kuntschner, H., Rejkuba, M., et al. 2010, *A&A*, 510, A19+  
 Maraston, C. 2005, *MNRAS*, 362, 799  
 Maraston, C., Daddi, E., Renzini, A., et al. 2006, *ApJ*, 652, 85  
 Marigo, P. & Girardi, L. 2007, *A&A*, 469, 239  
 Marigo, P., Girardi, L., Bressan, A., et al. 2008, *A&A*, 482, 883  
 Mateo, M. L. 1998, *ARA&A*, 36, 435  
 Otto, E., Green, P. J., & Gray, R. O. 2011, *ApJS*, 196, 5  
 Robin, A. C., Reylé, C., Derrière, S., & Picaud, S. 2003, *A&A*, 409, 523  
 Scalo, G. M. & Miller, G. E. 1981, *AJ*, 248, 65  
 Schlegel, D. J., Finkbeiner, D. P., & Davis, M. 1998, *ApJ*, 500, 525  
 Sibbons, L. F., Cioni, M.-R. L., Irwin, M., & Rejkuba, M. 2010, ArXiv:1011.4464  
 Soubiran, C., Le Campion, J.-F., Cayrel de Strobel, G., & Caillo, A. 2010, *A&A*, 515, 111  
 Tolstoy, E., Irwin, M. J., Cole, A. A., et al. 2001, *MNRAS*, 327, 918  
 Turnshek, D. E., Turnshek, D. A., Craine, E. R., & Boeshaar, P. C. 1985, An atlas of digital spectra of cool stars (Tucson, Arizona 85745: Western Research Company)  
 Venn, K. A., Lennon, D. J., Kaufer, A., et al. 2001, *ApJ*, 547, 765  
 Ventura, P. & Marigo, P. 2010, *MNRAS*, 408, 2476  
 Weldrake, D. T. F., de Block, W. J. G., & Walter, F. 2003, *MNRAS*, 340, 12  
 Zacharias, N., Monet, D. G., Levine, S. E., et al. 2005, *SIMBAD*, 1297

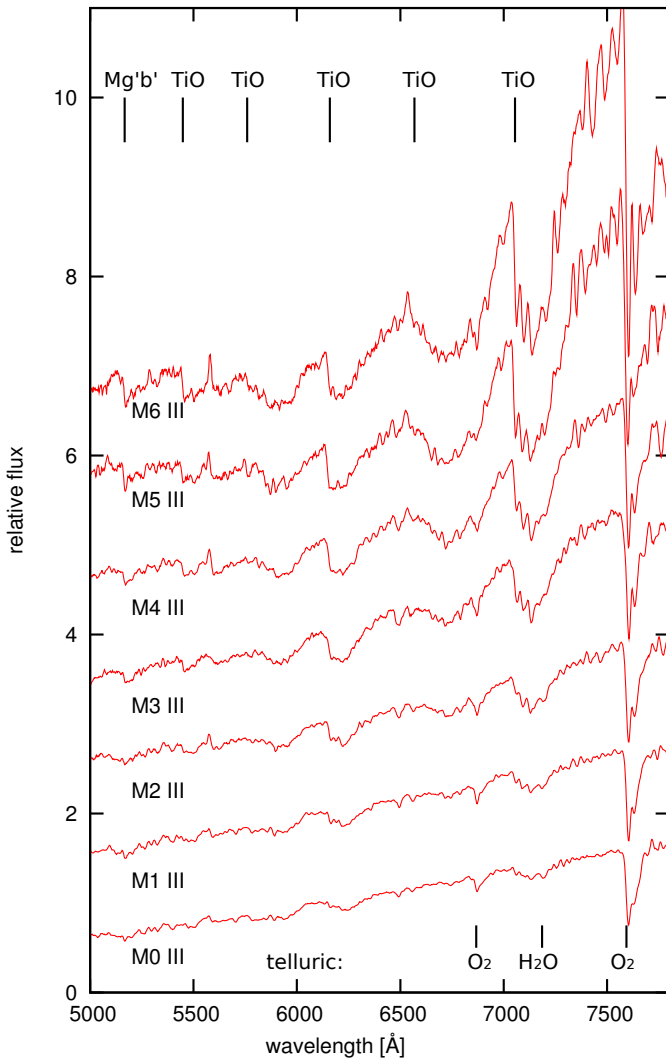


**Fig. A.1.** Full sample of average spectra for different spectral types giants according to our classification. The blue edge positions of some of the strongest TiO bands are shown with black lines as well as some telluric bands. The spectra are shifted along the y-axis with an arbitrary constant for presentation purposes.

**Appendix A: Full sample of M-type average spectra for giant and dwarf stars**

**Appendix B: Full spectrophotometric catalogue**

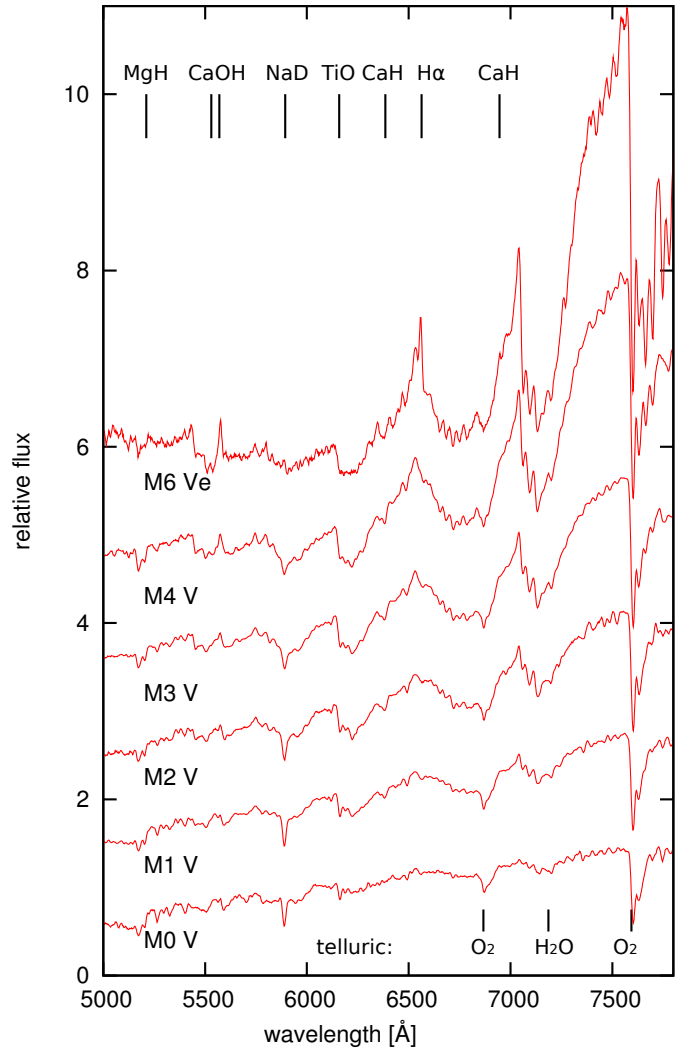


**Fig. A.2.** Full sample of average spectra for different spectral types dwarfs according to our classification. The positions of some of the most characteristic features as well as some telluric bands are shown with black lines. Among these are the sodium doublet (not resolved), the MgH, and the CaH bands. The spectra are shifted along the y-axis with an arbitrary constant for presentation purposes.

**Table B.1.** Full spectrophotometric catalogue.

ID	X [px]	Y [px]	RA [deg]	DEC [deg]	r [deg]	R [mag]	J [mag]	H [mag]	K [mag]	Sp. Cl. photometry	Sp. Cl. spectroscopy	Quality flag
94208	219.732	1679.789	296.349976	-14.828187	0.1121527	19.772	17.877	17.0450	16.898	M	M1III	4
94979	330.734	1801.989	296.357117	-14.834526	0.1206048	19.509	17.528	16.7200	16.515	Mca	M1III	4
96968	608.073	1462.655	296.337067	-14.850516	0.1073543	18.978	16.924	16.0800	15.693	C	C5.5	5
97590	696.476	1751.644	296.354126	-14.855531	0.1249199	19.406	17.334	16.5210	16.218	M	C5.5	5
98478	830.038	930.973	296.306183	-14.863027	0.08862444	23.062	17.451	16.2840	15.489	C	-	4
99641	1001.033	2013.256	296.369537	-14.872893	0.1464667	20.196	17.025	15.9710	15.317	C	C6.5	5
100035	1068.920	652.043	296.289734	-14.876258	0.08785845	17.078	17.404	16.5370	15.991	C	-	4
101911	1355.722	158.286	296.260742	-14.892557	0.09137722	20.645	17.952	17.1530	16.985	M	M	4
77311	48.431	1099.388	296.316101	-14.679276	0.1453135	19.438	17.443	16.6010	16.179	C	C6.5	5
79509	475.349	2029.313	296.371155	-14.703938	0.1641518	20.219	18.079	17.1980	16.991	M	M1III	5
83906	1226.993	1566.500	296.343781	-14.746560	0.1178242	21.667	17.437	16.5320	16.128	C	C5.5	5
85530	1462.654	1902.611	296.363739	-14.759742	0.1306686	23.344	16.528	15.5650	14.986	C	C5.5	5
85885	1506.260	2089.456	296.374664	-14.762603	0.1401522	22.981	17.504	16.5860	16.355	M	M4III	5
88539	1880.543	1058.628	296.313934	-14.783896	0.07590062	22.971	17.388	16.3590	15.668	C	C5.5	4
77230	140.325	1975.243	296.193542	-14.678253	0.1337262	20.206	17.488	16.4980	16.071	C	C5.5	5
78095	311.616	1734.144	296.179352	-14.688039	0.1306334	19.813	17.241	16.3500	16.076	M	C5.5	5
78871	459.932	2256.131	296.210236	-14.696464	0.1111891	21.556	16.949	16.3370	15.919	M	dM5 e	5
79224	532.454	1875.599	296.187653	-14.700607	0.1156495	21.826	17.792	17.0730	16.777	M	M6.5III	5
79511	589.745	1921.752	296.166718	-14.703956	0.1239035	20.233	17.724	16.8900	16.697	M	M1III	4
80764	832.120	1828.010	296.184784	-14.717754	0.1022478	20.280	17.435	16.4590	16.039	C	C5.5	5
81015	879.108	1219.159	296.148743	-14.720551	0.1237123	20.331	18.060	17.2540	17.066	M	M1III	5
81290	923.831	1041.148	296.138214	-14.723130	0.1301111	20.327	17.227	16.1880	15.542	C	C6.5	5
82246	1076.064	1643.366	296.173828	-14.731837	0.09789109	20.061	17.335	16.5430	16.299	M	M4III	6
83467	1267.180	2155.227	296.204193	-14.742633	0.07085879	18.691	15.048	14.1730	13.874	M	M6III	6
83752	1310.298	1599.732	296.171265	-14.745203	0.09053338	20.500	18.020	17.2280	16.970	M	C5.5	5
84020	1354.477	1830.278	296.185242	-14.747572	0.07863506	23.015	17.622	16.7990	16.588	M	dM	5
85975	1628.458	2046.414	296.197662	-14.763362	0.0587216	20.414	17.175	16.2550	15.536	C	C5.5	5
86798	1753.719	2238.658	296.208893	-14.769947	0.04610623	24.466	17.025	16.2010	15.758	C	C6.5	5
88152	1934.647	2076.698	296.199615	-14.780900	0.04676038	20.389	18.414	17.4210	17.201	C	M2III	5
88716	2021.618	2204.011	296.206879	-14.785284	0.03828439	19.733	18.082	17.2090	17.074	M	C5.5	5
93532	99.508	1716.032	296.178833	-14.822721	0.06469996	20.139	17.330	16.4750	16.210	M	SIII	5
93858	143.567	1738.309	296.180084	-14.825297	0.0643363	19.755	17.231	16.3660	15.897	C	C5.5	6
94446	230.224	2278.535	296.212219	-14.830112	0.03894694	20.872	17.270	16.3430	16.036	Cca	C8.2	5
94947	300.292	1631.935	296.173828	-14.834276	0.07354362	20.655	18.015	17.1510	16.987	Mca	M1III	5
95293	347.628	1413.000	296.160797	-14.836968	0.08655488	20.626	18.027	17.3700	17.092	Mca	dM3	6
95728	403.469	2278.123	296.212219	-14.840272	0.04650028	20.195	17.982	17.2200	16.969	Mca	M1III	5
96027	446.237	1980.717	296.194489	-14.842676	0.06054405	20.110	17.014	16.1110	15.568	C	C5.5	6
96655	534.901	2107.292	296.202057	-14.847754	0.05873197	20.336	17.178	16.1740	15.577	Cca	C5.5	6
97310	630.525	1483.251	296.164886	-14.853178	0.09058697	20.933	17.217	16.0280	15.151	C	C5.5 e	5
97913	716.647	1730.092	296.179565	-14.858191	0.08199306	20.623	17.341	16.3750	15.818	C	C5.5	6
98241	766.439	1879.345	296.188385	-14.861088	0.0777808	20.347	17.551	16.5470	16.182	C	C5.5	6
98573	817.915	1354.279	296.157288	-14.863935	0.1029569	20.610	17.318	16.4730	16.265	M	S4III	5
99143	899.102	1716.438	296.178772	-14.868636	0.08985176	20.434	17.478	16.4020	15.788	C	C5.5	5
99429	941.077	2155.420	296.204865	-14.871100	0.07652162	19.485	16.935	16.1020	15.807	M	C3.2	4
99831	1001.368	2176.731	296.206085	-14.874577	0.07907305	20.500	18.145	17.3370	17.039	M	M1III	5
100207	1059.988	1544.010	296.168549	-14.877820	0.103556	20.499	17.222	16.1570	15.564	C	C5.5	6
100545	1120.211	656.699	296.116089	-14.881053	0.146717	20.608	17.310	16.2500	15.450	C	C5.5	6
100929	1170.884	1554.526	296.169189	-14.884176	0.1077872	18.537	15.852	15.0160	14.782	M	M3III	6
101207	1213.494	1965.984	296.193604	-14.886700	0.09561194	20.821	18.299	17.3730	17.215	M	M1III	4
101866	1317.354	261.889	296.092773	-14.892178	0.1724127	20.724	17.214	16.1570	15.608	C	C6.5	5
102365	1382.647	2199.900	296.207458	-14.896397	0.09869482	20.202	17.393	16.5830	16.197	C	C5.5	5
102622	1429.550	698.842	296.118591	-14.898730	0.1548093	19.469	16.894	16.0340	15.732	M	C5.5	6
102922	1469.457	1946.731	296.192444	-14.901339	0.1091068	19.995	17.672	16.7560	16.644	M	M1III	5
103170	1512.781	637.136	296.114899	-14.903462	0.1606384	21.228	18.059	17.3320	17.124	M	dM	5
103686	1589.714	1849.405	296.186646	-14.908154	0.1178013	20.290	17.764	16.8700	16.708	M	M2III	5
105632	1911.998	2186.210	296.206696	-14.926620	0.1277681	20.623	16.997	15.8610	15.147	C	C6.5 e	5
106121	1995.065	1133.199	296.144318	-14.931097	0.1598977	20.290	17.520	16.6130	16.411	M	S4III	5
93464	115.145	1545.581	296.342345	-14.822172	0.1034667	19.982	17.481	16.5810	16.401	M	M3III	6
93781	159.119	1367.898	296.331849	-14.824688	0.09370232	19.914	18.029	17.0300	16.852	M	M1III	5
94073	198.307	1365.637	296.331716	-14.826927	0.09410673	19.681	17.657	16.8000	16.693	M	M0III	4
94429	251.999	1710.987	296.351776	-14.830035	0.1143249	19.629	17.677	16.9310	16.712	Mca	C8.2	5
94986	330.474	1607.357	296.345673	-14.834577	0.109602	19.646	17.219	16.3410	15.898	Cca	C5.5	5
95355	381.519	188.258	296.262573	-14.837487	0.04053589	21.772	17.440	16.6190	16.297	Mca	-	4
96598	552.443	1569.942	296.343445	-14.847301	0.1118206	19.728	17.905	17.0470	16.885	Mca	M0III	5
97225	643.947	1948.517	296.365814	-14.852487	0.1344904	19.955	17.293	16.2590	15.570	C	C5.5	6
97567	692.912	1625.477	296.346741	-14.855356	0.118171	19.721	17.320	16.4810	16.022	C	C5.5	6
100023	1057.845	2118.620	296.375763	-14.876107	0.1534723	20.461	17.948	17.0280	16.819	M	M4III	6
100521	1140.994	1899.504	296.363129	-14.880856	0.1449505	20.763	17.439	16.5950	16.435	M	M	4
101802	1328.222	1947.256	296.365631	-14.891643	0.1530257	17.818	15.562	14.7120	14.318	C	M5III	6
102163	1381.521	181.820	296.261505	-14.894732	0.09366731	19.226	17.792	16.8330	16.802	M	M	4
103115	1528.656	1432.273	296.335785	-14.902986	0.1377446	22.048	17.233	16.4110	16.022	C	M	4
104988	1839.747	603.009	296.286987	-14.920337	0.1257777	20.379	16.908	16.0870	15.896	M	M4III	6
105583	1936.177	395.957	296.275116	-14.926181	0.1275145	17.681	18.321	17.4000	17.123	C	M	4
100901	1194.765	2204.951	296.380829	-14.883905	0.1616888	19.816	17.628	16.7630	16.596	M	M2III	6
77470	79.012	1424.934	296.335388	-14.681108	0.1547554	20.811	18.391	17.5060	17.091	C	C6.5	5
78605	300.450	1175.215	296.320587	-14.693704	0.1357911	20.496	18.135	17.2270	17.169	M	M4III	5
79960	565.862	723.431	296.293854	-14.708783	0.1086049	19.802	17.537	16.5730	16.344	C	C8.2	5
80354	632.794	1973.000	296.367828	-14.712914	0.1561492	19.776	17.585	16.7650	16.497	M	M1III	5
81804	893.125	2201.301	296.381348	-14.727878	0.1597525	19.818	17.516	16.6270	16.418	M	M4III	6
82163	951.905	1764.820	296.355621	-14.731111	0.1358754	20.880	18.112	17.4290	17.172	M	dM	4
83580	1183.490	576.054	296.285706	-14.743645	0.07489761	19.592	17.682	16.8610	16.682	M	M2III	6
86652	1624.801	181.656	296.262848	-14.768750	0.04120793	20.685	17.647	16.7960	16.637	M	C6.5	5
88480	1876.											













ID	X [px]	Y [px]	RA [deg]	DEC [deg]	r [deg]	R [mag]	J [mag]	H [mag]	K [mag]	Sp. Cl. photometry	Sp. Cl. spectroscopy	Quality flag
57732	827.898	708.120	296.954742	-14.473660	0.7866137	22.591	18.343	17.8040	17.385	M	K	3
57978	896.278	1725.470	297.014343	-14.477056	0.8397698	21.46	18.167	17.5550	17.215	M	dM	4
58422	1006.956	957.693	296.968933	-14.483230	0.7956201	20.872	17.727	17.0760	16.816	M	dM	4
59131	1188.569	1876.573	297.023346	-14.493817	0.8417642	21.156	18.165	17.5550	17.168	M	dM	4
60052	1366.221	1754.735	297.016083	-14.503956	0.8313085	21.259	18.178	17.6320	17.433	M	dM	4
60786	1487.377	1799.477	297.018768	-14.510902	0.8313443	20.503	18.148	17.6510	17.346	M	dM3	5
61414	1597.897	427.123	296.937805	-14.516788	0.7538383	19.436	17.791	17.1000	16.940	M	dM0	5
61782	1657.570	1600.655	297.006958	-14.520561	0.8169055	20.277	17.413	16.7880	16.564	M	dM3	5
62104	1705.797	1828.993	297.020477	-14.523369	0.8286481	20.379	18.044	17.3630	17.141	M	dM3	5
62393	1762.292	696.747	296.953674	-14.526256	0.7650582	20.050	18.052	17.4470	17.269	M	dM1.5	5
62691	1812.163	336.567	296.932526	-14.528950	0.7443886	18.610	16.632	15.9790	15.793	M	dM1.5	6
63105	1876.585	1788.570	297.018127	-14.533105	0.8231884	18.940	17.651	17.0460	16.895	M	dK7	5
63424	1938.155	1067.854	296.975586	-14.536401	0.7819996	20.393	17.165	16.6410	16.351	M	dM4.5	5
63663	1980.842	887.455	296.964935	-14.538761	0.7711843	18.523	16.722	16.0230	15.882	M	dM1.5	6
136956	256.335	1523.124	295.645844	-15.270988	0.7565274	21.027	18.097	17.5640	17.253	M	dM3.5	4
139836	857.547	1398.050	295.638458	-15.305284	0.78385	18.308	17.652	16.9110	16.703	M	dK	4
142268	1410.831	973.393	295.612732	-15.336275	0.8234864	18.072	17.830	17.1280	16.957	M	dK	4
142730	1509.938	1521.907	295.644928	-15.342483	0.8033628	17.846	17.427	16.7960	16.615	M	dK	4
143023	1590.810	614.538	295.591583	-15.346883	0.8464938	18.352	16.991	16.2760	15.991	M	dK	4
143950	1808.174	1065.145	295.618652	-15.359362	0.8341869	21.326	17.498	16.8920	16.726	M	dK	4
144255	1871.771	479.626	295.584229	-15.363297	0.8627058	18.206	17.197	16.5530	16.344	M	dK	4
128247	1040.452	1126.373	295.622314	-15.175920	0.7218132	20.969	18.314	17.5150	17.276	M	M	4
129250	1218.280	2169.862	295.683594	-15.186219	0.6758493	21.990	18.208	17.5960	17.426	M	dM	4
126166	668.011	2267.463	295.689667	-15.155052	0.6535705	24.553	17.736	16.7870	16.428	C	-	4
131608	1653.595	2241.736	295.688568	-15.211617	0.6865458	20.194	17.775	17.1530	16.833	M	dM0	4
123364	216.995	1359.148	295.460785	-15.123086	0.8427787	20.475	18.389	17.7120	17.401	M	dM	5
124511	445.084	1274.828	295.456573	-15.136149	0.8516953	18.275	17.643	16.9520	16.724	M	dM0	5
125420	625.915	1428.566	295.464996	-15.146566	0.8481089	19.330	17.472	16.7390	16.559	M	dM0	5
130615	1574.202	904.421	295.434204	-15.201089	0.8991058	19.391	16.736	16.0630	15.827	M	-	4
131365	1726.452	2073.666	295.503571	-15.209061	0.8412692	18.599	18.138	17.3880	17.182	M	dM0	5
137212	288.103	1754.533	295.485199	-15.273877	0.889908	19.066	17.789	16.9970	16.800	M	K7III	4
139197	703.094	593.642	295.416962	-15.297790	0.9606015	21.676	18.304	17.5610	17.378	M	dM	4